Development of discontinuous Galerkin methods for hyperbolic systems that preserve a curl or a divergence constraint

Vincent Perrier

Development of discontinuous Galerkin methods for hyperbolic systems that preserve a curl or a divergence constraint

Vincent Perrier
Team Cagire, INRIA Bordeaux Sud-Ouest.
Laboratoire de Mathématiques et de leurs applications
Bâtiment IPRA, Université de Pau et des Pays de l'Adour,
Avenue de l'Université, 64 013 Pau Cedex

May 6, 2024

Abstract

Some hyperbolic systems are known to include implicit preservation of differential constraints: these are for example the time conservation of the curl or the divergence of a vector that appear as an implicit constraint. In this article, we show that this kind of constraint can be easily conserved at the discrete level with the classical discontinuous Galerkin method, provided the right approximation space is used for the vectorial space, and under some mild assumption on the numerical flux. For this, we develop a discrete differential geometry framework for some well chosen piece-wise polynomial vector approximation space. More precisely, we define the discrete Hodge star operator, the exterior derivative, and their adjoints. The discrete adjoint divergence and curl are proven to be exactly preserved by the discontinuous Galerkin method under a small assumption on the numerical flux. Numerical tests are performed on the wave system, the two dimensional Maxwell system and the induction equation, and confirm that the differential constraints are preserved at machine precision while keeping the high order of accuracy.

Contents

1 Introduction

In this article, we are interested in the discrete conservation of differential constraints that appear implicitly in a hyperbolic system of conservation law. Suppose for example that a hyperbolic system includes a vectorial unknown $\mathbf{u}$ for which the conservation law is

$$\partial_t \mathbf{u} + \boldsymbol{\nabla} \cdot \overline{\mathbf{G}} = 0,$$

where $\overline{\mathbf{G}}$ is a matrix. If $\overline{\mathbf{G}}$ is proportional to the identity matrix, namely if a scalar function g exists such that $\overline{\mathbf{G}} = g\mathrm{I}_d$, then the conservation law becomes

$$\partial_t \mathbf{u} + \nabla g = 0,$$

and taking the curl of the equation on $\mathbf{u}$ gives formally the conservation of the curl of $\mathbf{u}$:

$$\partial_t \left(\nabla \times \mathbf{u}\right) = \nabla \times \left(\partial_t \mathbf{u}\right) = -\nabla \times \left(\nabla g\right) = 0.$$

In the same manner, if $\overline{\mathbf{G}}$ is antisymmetric, then the divergence of $\mathbf{u}$ is constant.

This kind of implicit differential constraint appears in a large number of systems including incompressible Navier-Stokes system, Maxwell system, magnetohydrodynamics (MHD), and wave and elastodynamic problems written in first order formulation. Preservation of such constraints at the discrete level has been addressed by several strategies, which can be gathered as

- **Staggering of unknowns.** Staggering unknowns consists in non collocated distribution of unknowns, for example in defining scalar unknowns in each cells, and vector unknowns in the sides of the mesh. The staggering of unknowns was proposed for the incompressible Navier-Stokes system in the MAC scheme [44], and for the Yee scheme [68] for Maxwell equations, see also [5, 6, 7] for the MHD system. Staggering of unknowns has been the object of a huge body of papers, including see e.g. [52, 51, 25, 28, 26] for the analysis of the MAC scheme. Among the large family of staggered schemes enters also the work on compatible

discretization [41, 46], or the staggered discontinuous Galerkin method [61]. This includes also the work on discrete exterior calculus with finite elements, including theoretical work around the Hodge Laplacian and its well posed mixed formulation [2, 3, 4], see also the book [1], work on electromagnetism [15, 16, 17, 39, 40] and discretization of the Lie-advection equation [36, 37, 38] and application [53]. Staggered discretizations were extended also to polytopal meshes, mainly for incompressible systems see e.g. the virtual element method [10], the Hybrid High order (HHO) methods [22] or the Compatible Discrete Operators (CDO) method [12, 13, 47]. The main difficulty of staggered discretizations for nonlinear hyperbolic systems is to keep a correct definition of the conservation; especially, keeping conservation while shock-limiting staggered data is challenging.

- **Projection method.** The projection method was mainly used for divergence cleaning in [18] for the MHD system and in [11] for incompressible Navier-Stokes system. The projection method is a predictor-corrector method. Suppose for example that the divergence of a vector $\mathbf{v}$ should be preserved. Suppose also that a predictor step provided a candidate update for $\mathbf{v}^{n+1}$ of $\mathbf{v}^n$, but that the divergence is not preserved. Then a potential φ such that

$$\Delta\varphi = \nabla \cdot \left(\mathbf{v}^{n+1} - \mathbf{v}^n\right),$$

  may be computed. Then $\tilde{\mathbf{v}}^{n+1} := \mathbf{v}^{n+1} - \nabla\varphi$ is a projection of $\mathbf{v}^{n+1}$ for which the divergence is preserved. The main drawback of this method is the cost of the inversion of an elliptic system at each time step, and the definition of the boundary conditions for this elliptic system.

- **Generalized Lagrange Multiplier method.** This method, first developed in [49, 20] consists in considering the divergence to be preserved as an additional variable. Then an additional equation for this variable, and a relaxation process ensure that the divergence is asymptotically preserved. This method was extended to curl preservation in [23]. The difficulty with this system is its higher computational cost because of the additional variables, and the tuning of the numerical relaxation parameters.

Another category of method was especially designed for the conservation of the zero divergence of the magnetic field in the Maxwell system, the MHD system or the induction model system; these systems are slightly different from the ones previously discussed, because the divergence of the magnetic field is not directly preserved by the system. Instead, the divergence is solution of a conservative transport equation, so that an initially divergence free magnetic field is divergence free for all time. These two categories of methods are

- **the Godunov-Powell method.** This method consists in relying on the formulation of Godunov [30, 29] and Powell [55, 56] for the MHD equation, and in trying to control the divergence of the magnetic field [27, 48] (note however that the magnetic field is not divergence free, the aim of the method is only to keep this divergence "low").

- **Constrained Transport Method.** This method was originally proposed in [24] as an alternative of the Yee scheme [68], and under a staggered fashion. This method is based on staggered ideas, and in the Maxwell context, the challenge consists in the computation of a reliable staggered electric field based on a magnetic field that, still *may not be staggered*: indeed, in [65], several methods were compared, including different versions of the contrained transport method, and it was shown that the method can be collocated, see also [64, 63, 35]. Concerning the contrained transport method, we also refer to the review [62] and references therein, [66] for a high order constrained transport method based on spectral differences, and [42] for an extension to the preservation of a curl.

Apart from these schemes that are especially designed for preserving exactly a discrete curl or a discrete divergence, some collocated numerical schemes seem to be *naturally* able to preserve these constraints. This is for example the case of numerical schemes developed within the low Mach

number community [21, 32, 33, 43], which inspired the present article. Even if these references do no state any relation with curl preservation, they are actually preserving a curl that will be defined in this article. Another family of schemes that seem to preserve exactly divergence or curl constraints are node based numerical schemes, see e.g. [14] for the divergence preservation or [8, 9] for curl preservation. Considering their stencils, these schemes seem to have a close relationship with [63, 42], which are based on the unstaggered constrained transport method. In this article, we wish to develop discontinuous Galerkin methods that *naturally* preserve a divergence or a curl *exactly*, which match with [21, 32, 33, 43] for straight triangular meshes but which differ on quadrangular meshes because we use alternative approximation space for vectors, proposed in [54].

This article is organized as follows. In section 2, the basics of the two-dimensional de-Rham complex is recalled. The classical conformal finite element approximation based on the continuous / Nédélec / Raviart-Thomas complex is recalled, and the nonconforming approach proposed in [54] is reviewed. The classical discrete operators (Hodge-star operator, codifferentials) are then defined in section 3. Based on these approximation spaces and matching discrete operators, we prove in section 4 that the classical discontinuous Galerkin method is able to preserve a curl or a divergence constraint provided the right approximation space is used, and under a small hypothesis regarding the diffusion direction of the numerical flux. Then in section 5, we explain how the numerical scheme can be also extended to the induction equation; we especially prove that if the vector field is correctly initialized, then it is divergence free (still in the adjoint sense) for all time. In section 6, the numerical scheme is tested for the preservation of a divergence with the two dimensional Maxwell system, the preservation of a curl with the two dimensional first order formulation of the wave system, and the preservation of the divergence free field with the induction equation. In this numerical section, convergence tests are also performed. This article finishes with the conclusion in section 7.

2 Continuous and discrete de-Rham complex

2.1 Differential forms and the de-Rham complex

2.1.1 Space of alternate forms

Differential forms are a powerful tool which may be used also in the partial differential equations context for exhibiting and analyzing geometrical structure of these equations.

This theory starts with alternate k-multilinear forms on $\mathbb{R}^2$ that we denote by Λ^k. In this paper, continuous and discrete linear forms will be denoted by gothic letters, e.g. $\mathfrak{f}$, $\mathfrak{u}$ or $\mathfrak{g}$. Scalars will be denoted by italic small letters (e.g. f, g), and vectors by roman bold letters (e.g. $\mathbf{u}$, $\mathbf{v}$). On $\mathbb{R}^2$, Λ^k is the null space for $k \geq 3$. For $0 \leq k \leq 2$, we have:

- Λ^0 is the set of 0-linear forms on $\mathbb{R}^2$; a 0 multilinear form $\mathfrak{f} \in \Lambda^0$ is completely determined by a constant f:
$$\mathfrak{f}() = f.$$
- Λ^1 is the set of 1-linear forms. They are usually represented in two manner
  - Either by the scalar product by a vector $\mathbf{u}$:
$$\forall \mathfrak{u} \in \Lambda^1 \quad \exists! \mathbf{u} \in \mathbb{R}^2 \quad \forall \mathbf{v}_1 \in \mathbb{R}^2 \qquad \mathfrak{u}(\mathbf{v}_1) = \mathbf{u} \cdot \mathbf{v}_1, \tag{1}$$
  - or by the determinant with a vector $\tilde{\mathbf{u}}$:
$$\forall \mathfrak{u} \in \Lambda^1 \quad \exists! \tilde{\mathbf{u}} \in \mathbb{R}^2 \quad \forall \mathbf{v}_1 \in \mathbb{R}^2 \qquad \mathfrak{u}(\mathbf{v}_1) = \det(\mathbf{v}_1, \tilde{\mathbf{u}}). \tag{2}$$
    Note that $\mathbf{u} \cdot \mathbf{v}_1 = \det(\mathbf{v}_1, \tilde{\mathbf{u}})$ if and only if $\tilde{\mathbf{u}}$ is the image of $\mathbf{u}$ by the $\pi/2$ rotation which we denote by a $\perp$ exponent: $\tilde{\mathbf{u}} = \mathbf{u}^\perp$.

$\mathfrak{u}$	$\mathfrak{v}$	Proxy $(\mathfrak{u} \wedge \mathfrak{v})$
Λ^0	Λ^0	uv
Λ^0	Λ^1	$u\mathbf{v}$
Λ^0	Λ^2	uv
Λ^1	Λ^1	$\det(\mathbf{u}, \mathbf{v})$

Table 1: Expression of the effect of the exterior product on the scalar and vector proxies. This effect is independent of the choice of the proxy for Λ^2 ((1) or (2)).

- Λ^2 is the set of alternate 2-linear forms. It is known that all the alternate 2-linear forms are proportional to the determinant:

$$\forall \mathfrak{f} \in \Lambda^2 \quad \exists! f \in \mathbb{R} \quad \forall \mathbf{v}_1, \mathbf{v}_2 \in \mathbb{R}^2 \qquad \mathfrak{f}(\mathbf{v}_1, \mathbf{v}_2) = f \det(\mathbf{v}_1, \mathbf{v}_2).$$

The choice of the proxy (1) or (2) will have an impact on the whole list of operators that will be defined. We will denote by Proxy the proxy of a linear form when (1) is chosen, and by $\text{Proxy}^\perp$ the proxy of a linear form when (2) is chosen. A large number of operators on linear forms will be introduced all along this article, and the matches between operators on proxies and operators on linear forms is summarized in Appendix A. The scalar f is called the *scalar proxy* of the alternate 0 or 2 linear form $\mathfrak{f}$, whereas the vectors $\mathbf{u}$ or $\tilde{\mathbf{u}}$ are called the *vector proxies* of the alternate 2-linear form $\mathfrak{u}$. Several additional tools are needed on these sets of alternate linear forms:

- The *exterior product* $\wedge$ is defined in general as [19, Chap. 1.4]

$$\begin{array}{rcl} \wedge : \Lambda^i \times \Lambda^j & \longmapsto & \Lambda^{i+j} \\ (\mathfrak{u}, \mathfrak{v}) & \longmapsto & \mathfrak{u} \wedge \mathfrak{v}, \end{array}$$

  with

$$\mathfrak{u} \wedge \mathfrak{v}(\mathbf{v}_1, \ldots, \mathbf{v}_i, \mathbf{v}_{i+1}, \ldots \mathbf{v}_{i+j}) = \sum_{\sigma \in \mathscr{A}_{i+j}} \varepsilon(\sigma) \mathfrak{u}\left(\mathbf{v}_{\sigma(1)}, \ldots, \mathbf{v}_{\sigma(i)}\right) \mathfrak{v}\left(\mathbf{v}_{\sigma(i+1)}, \ldots, \mathbf{v}_{\sigma(i+j)}\right),$$

  where $\mathscr{A}_{i+j}$ is the set of $(i+j)$-permutations such that

$$\sigma(1) < \cdots < \sigma(i) \qquad \text{and} \qquad \sigma(i+1) < \cdots < \sigma(i+j),$$

  and $\varepsilon(\sigma)$ is the signature of the permutation σ. The exterior product ensures $\mathfrak{u} \wedge \mathfrak{v} = (-1)^{ij} \mathfrak{v} \wedge \mathfrak{u}$. The effect of the exterior product on the proxies is recalled in Table 1.

- A *scalar product* may be defined on Λ^k, which in our case is equivalent to the classical scalar or vector scalar product on the proxies, and which we denote by $\langle \cdot | \cdot \rangle_{\Lambda^k}$

- Last, we denote by $\mathfrak{vol}$ the volume form, the element of Λ^2 such that

$$\forall \mathbf{v}_1, \mathbf{v}_2 \in \mathbb{R}^2 \qquad \mathfrak{vol}(\mathbf{v}_1, \mathbf{v}_2) := \det(\mathbf{v}_1, \mathbf{v}_2),$$

  and we define the *Hodge-star* operator, that will be denoted by $\bigstar_{\{k\}}$, as the operator from Λ^k to Λ^{2-k} such that

$$\forall \mathfrak{u} \in \Lambda^k \quad \forall \mathfrak{v} \in \Lambda^{2-k} \qquad \mathfrak{u} \wedge \mathfrak{v} = \left\langle \bigstar_{\{k\}}(\mathfrak{u}) \middle| \mathfrak{v} \right\rangle_{\Lambda^{2-k}} \mathfrak{vol}.$$

  Concerning the proxies, $\bigstar_{\{0\}}$ and $\bigstar_{\{2\}}$ are the identity, whereas $\bigstar_{\{1\}}$ is the $\pi/2$ rotation.

2.1.2 Space of differential forms and the de-Rham complex

We denote by $C^\infty\Lambda^k$ the space of differential k-forms, namely the functions $\mathbb{T}^2 \mapsto \Lambda^k$ that are infinitely differentiable, where $\mathbb{T}^2$ is the two-dimensional torus. It is equipped with the norm

$$\langle \mathfrak{u}|\mathfrak{v}\rangle_{L^2\Lambda^k} := \int_{\mathbb{T}^2} \langle \mathfrak{u}|\mathfrak{v}\rangle_{\Lambda^k}.$$

If $\mathfrak{u} \in C^\infty\Lambda^k$, then its derivative $\mathfrak{u}'$ is a linear application from $\mathbb{R}^2$ to Λ^k, which may be seen as a $(k+1)$-linear application. Denoting by

$$\partial_{\mathbf{v}_j}\mathfrak{u} := \mathfrak{u}' \cdot \mathbf{v}_j,$$

the *exterior derivative* [19, Chap. 2.3] d^k is defined as

$$\begin{array}{rccc} \mathrm{d}^k : & C^\infty\Lambda^k & \longmapsto & C^\infty\Lambda^{k+1} \\ & \mathfrak{u} & \longmapsto & \mathrm{d}^k\mathfrak{u}, \end{array}$$

with

$$\left(\mathrm{d}^k\mathfrak{u}\right)(\mathbf{v}_1,\dots,\mathbf{v}_{k+1}) = \sum_{j=1}^{k+1}(-1)^{j-1}\partial_{\mathbf{v}_j}\left(\mathbf{v}_1,\dots\mathbf{v}_{j-1},\mathbf{v}_{j+1}\dots,\mathbf{v}_k\right).$$

Denoting by ∇ the vector operator $(\partial_x,\partial_y)^T$, then

- If the choice of proxy is (1), then d^0 is ∇, whereas d^1 is $\nabla^\perp\cdot$.
- If the choice of proxy is (2), then d^1 is $\nabla^\perp$, whereas d^1 is $-\nabla\cdot$.

Regarding the relations between the $\pi/2$ rotation and the different differential operators, we wish to recall the following relations that will be useful in section 3:

$$\left\{\begin{array}{l} \nabla^\perp\cdot\mathbf{u} = -\nabla\cdot\mathbf{u}^\perp \\ \nabla\cdot\left(\mathbf{u}^\perp\right) = -\nabla^\perp\cdot\mathbf{u}, \\ \mathbf{u}\cdot\nabla^\perp f = -\mathbf{u}^\perp\cdot\nabla f. \end{array}\right.$$

Last, we denote by δ^k the *coderivative* which are defined in two dimensions as

$$\delta^1 := -\bigstar_{\{2\}}\mathrm{d}^1\bigstar_{\{1\}}, \tag{3}$$

and

$$\delta^2 := -\bigstar_{\{1\}}\mathrm{d}^0\bigstar_{\{2\}}. \tag{4}$$

Concerning the proxies, the δ operators are

- If the choice of proxy is (1), then δ^2 is $\left(-\nabla^\perp\right)$, whereas δ^1 is $(-\nabla\cdot)$.
- If the choice of proxy is (2), then δ^2 is ∇, whereas δ^1 is $\left(-\nabla^\perp\cdot\right)$.

$C^\infty\Lambda^k$ may be equipped with the graph norm $\|\cdot\|_k + \|\mathrm{d}^k\cdot\|_{k+1}$, and the closure of $C^\infty\Lambda^k$ is denoted by $H\Lambda^k$. This gives rise to a complex similar to the de-Rham complex, but with Sobolev spaces $H\Lambda^k$, called *Hilbert complex* [1, Chapter 4].

In Figure 1, the two-dimensional Hilbert complex was written, both in terms of differential forms spaces $H\Lambda^k$, and in terms of their vector proxies. A fundamental result on the de-Rham complex, which holds also for the Hilbert complex, is the link between the dimension of the cohomology groups and the Betti numbers[34], which are characteristic of the topology of the domain:

$$\left\{\begin{array}{l} b_0 = \dim\left(\ker\nabla\right), \\ b_1 = \dim\left(\ker\left(\nabla^\perp\cdot\right)/\operatorname{Range}\left(\nabla\right)\right), \\ b_2 = \dim\left(L^2/\operatorname{Range}\left(\nabla^\perp\cdot\right)\right). \end{array}\right. \tag{5}$$

In our case, on $\mathbb{T}^2$, the Betti numbers are $b_0 = b_2 = 1$ and $b_1 = 2$.

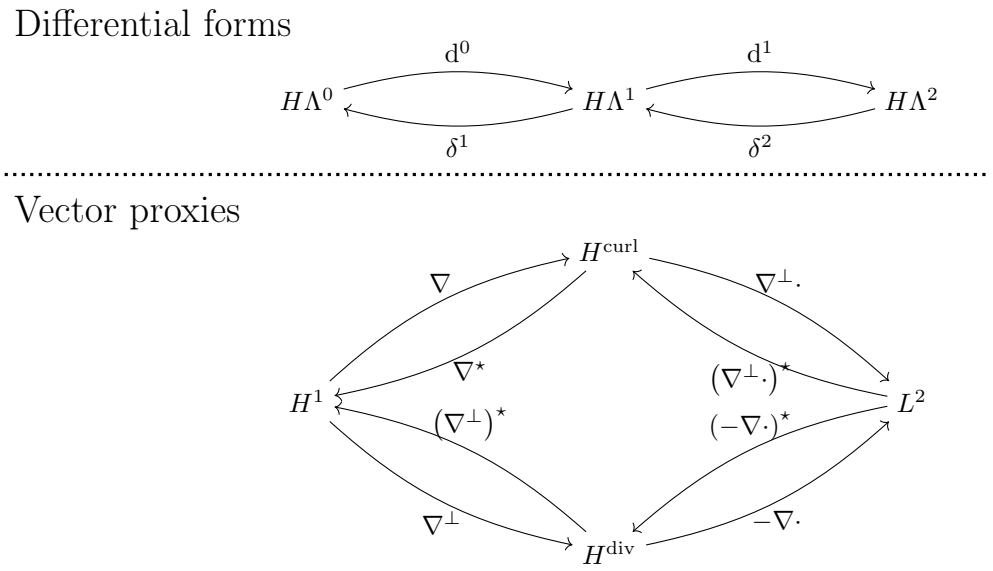

Figure 1: Two dimensional Hilbert complex. On the top, the differential forms version, with the exterior differential d and the codifferential δ. On the bottom part, the vector proxy version, with the different choices of proxy: (1), leading to the complex $\nabla/\left(\nabla^\perp\cdot\right)$ and (2), leading to the complex $\nabla^\perp/\left(-\nabla\cdot\right)$ versions, and their adjoints. The Figure can be also read column-wise, for example the space of differential forms $H\Lambda^1$ matches with H^{curl} or H^{div} depending on the choice of proxy representation of the linear forms, and the exterior differential d^0 matches with ∇ or $\nabla^\perp$ depending on the choice of proxy.

2.2 The discrete case

2.2.1 The classical conformal discrete de-Rham complex

From an approximation point of view, the study of discrete counterpart of the Hilbert complex of Figure 1 has been an intensive research topic over the last forty years, including the work of Whitney [67], Bossavit and Hiptmair on electromagnetism [15, 16, 17, 40], and the work on formalization of Arnold and collaborators of finite element exterior calculus [2, 3] which led to the reference book [1]. The classical conformal discrete counterpart of the de-Rham diagram of Figure 1 relies on the continuous/Nédélec/Raviart-Thomas complex [4, 57, 58, 50], where H^1 is replaced by the continuous finite elements $\mathbb{P}_{k+1}$, H^{div} by the two-dimensional Raviart-Thomas approximation space $\mathbb{RT}_k$, H^{curl} by the two-dimensional Nédélec approximation space $\mathbb{N}_k$, and L^2 by the discontinuous Galerkin approximation space $\mathrm{d}\mathbb{P}_k$, in which a key property from the preservation point of view relies on the equalities (5) which hold also at the discrete level.

2.2.2 Some complexes involving a discrete discontinuous space for velocities

We begin by providing some definitions on the mesh we are working on. The domain $\mathbb{T}^2$ is divided into a set of cells $\mathcal{C}$. The set of sides of the mesh is denoted by $\mathcal{S}$. Each side of the mesh is oriented, and with respect to a given side $S \in \mathcal{S}$, the left cell is the one for which the canonical normal is outgoing, whereas the right cell is the one in which the canonical normal is ingoing. The *jump* of a scalar f that is continuous on the cells and discontinuous across the faces is defined as

$$\forall S \in \mathcal{S} \qquad [\![f]\!]_S := f_L - f_R,$$

where f_L is the value on the left cell and f_R is the value on the right cell.

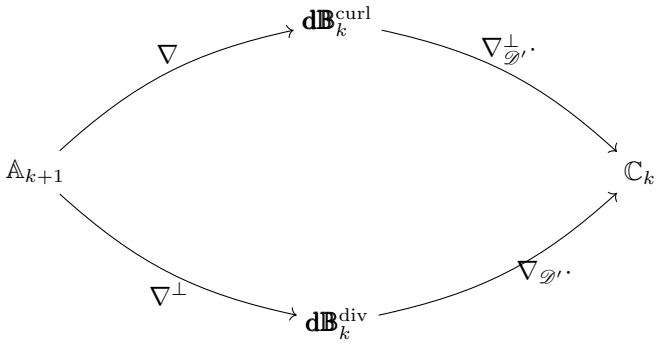

Figure 2: Two dimensional discrete de-Rham complex on the proxies proposed in [54]. The approximation space $\mathbb{A}_{k+1}$ is always a continuous finite element approximation space, namely $\mathbb{P}_{k+1}$ for triangles and $\mathbb{Q}_{k+1}$ for quadrangles. Depending on the properties needed, the choice of approximation space for $\mathbf{d}\mathbb{B}_k^{\mathrm{curl}}$ and $\mathbf{d}\mathbb{B}_k^{\mathrm{div}}$ may be very diverse. As the spaces $\mathbf{d}\mathbb{B}_k^{\mathrm{curl}}$ and $\mathbf{d}\mathbb{B}_k^{\mathrm{div}}$ include discontinuous functions, the application of the exterior derivative in the distribution sense (operators $\nabla^{\perp}_{\mathscr{D}'}\cdot$ and $\nabla_{\mathscr{D}'}\cdot$) includes the classical derivative located on the cells and the contribution of the normal or tangential jumps multiplied by a Dirac distribution located on the sides of the mesh. Therefore $\mathbb{C}_k$ appears as a Cartesian product of a cell-based finite element space and a side-based finite element space.

Recently, it was proposed to relax the continuity constraints induced by the conformal hypothesis [45]. Contrarily to the classical conformal approximation, the approximation of the vector spaces H^{curl} and H^{div} proposed in [45] are completely discontinuous, without any hypothesis on the continuity of the normal component (which holds for $\mathbb{RT}$) or the tangential component (which holds for $\mathbb{N}$). This idea was extended in [54] for finding basis with fewer degrees of freedom. The different approximation space for vectors proposed in [54] will be denoted by $\mathbf{d}\mathbb{B}_k^{\mathrm{div}}$ and $\mathbf{d}\mathbb{B}_k^{\mathrm{curl}}$. In this case, the classical derivation operators cannot be applied to these approximation space, and the derivative in the sense of distributions is used instead

$$\forall \mathbf{u} \in \mathbf{d}\mathbb{B}_k^{\mathrm{div}} \qquad \nabla_{\mathscr{D}'}\cdot\mathbf{u} := \begin{cases} \forall C \in \mathcal{C} & \left(\nabla_{\mathscr{D}'}\cdot\mathbf{u}\right)^C := \nabla\cdot\mathbf{u} \\ \forall S \in \mathcal{S} & \left(\nabla_{\mathscr{D}'}\cdot\mathbf{u}\right)^S := -\left[\!\left[\mathbf{u}\cdot\mathbf{n}\right]\!\right]. \end{cases}$$

and

$$\forall \mathbf{u} \in \mathbf{d}\mathbb{B}_k^{\mathrm{curl}} \qquad \nabla^{\perp}_{\mathscr{D}'}\cdot\mathbf{u} := \begin{cases} \forall C \in \mathcal{C} & \left(\nabla^{\perp}_{\mathscr{D}'}\cdot\mathbf{u}\right)^C := \nabla^{\perp}\cdot\mathbf{u} \\ \forall S \in \mathcal{S} & \left(\nabla^{\perp}_{\mathscr{D}'}\cdot\mathbf{u}\right)^S := \left[\!\left[\mathbf{u}^{\perp}\cdot\mathbf{n}\right]\!\right]. \end{cases}$$

We see that the image of the operators $(\nabla_{\mathscr{D}'}\cdot)$ and $\left(\nabla^{\perp}_{\mathscr{D}'}\cdot\right)$ is in a Cartesian product of cell space and face space, that we will denote in general $\mathbb{C}_k$. In [54], several such vectorial approximation spaces were proposed, for which the *harmonic gap property* [1, Chap. 5.2.3], which may be summarized as

Definition 1 (Harmonic gap property)**.** *A discrete diagram ensures the* harmonic gap property *if the discrete and continuous cohomology spaces are isomorphic, which induces that* (5) *holds.*

was proven on $\mathbb{T}^2$. The proposed approximation spaces may all be put in the diagram of Figure 2. In [54], the following approximation spaces were proposed; the first family is based on the conformal case, whereas the two other proposed approximation spaces are optimal in the number of degrees of freedom.

1. **Approximation spaces directly based on discontinuous versions of Raviart-Thomas/Nédélec finite elements.** In this version of the discontinuous spaces, proposed in [45], the polynomial basis are exactly the same as for the conformal approximation on each

cell, but all the continuity constraints are relaxed. These spaces were denoted by $\mathrm{d}\mathbb{RT}_k$ and $\mathrm{d}\mathbb{N}_k$. This leads to

$$\mathbb{C}_k = \mathrm{d}\mathbb{P}_k(\mathcal{C}) \times \mathrm{d}\mathbb{P}_k(\mathcal{S}),$$

for triangular meshes and to

$$\mathbb{C}_k = \mathrm{d}\mathbb{Q}_k(\mathcal{C}) \times \mathrm{d}\mathbb{P}_k(\mathcal{S}),$$

for quadrangular meshes. These approximation space work fine, but some degrees of freedom are useless for ensuring the harmonic gap property. Also the Raviart-Thomas/Nédélec finite element basis should be generated which is not always straightforward on triangular meshes.

2. **Optimal approximation spaces on triangles.** On triangles, the classical approximation space for vectors, namely the one obtained by tensorizing the classical approximation space for scalars can be put in the diagram Figure 2, as addressed in [54]; in this case, $\mathbf{d}\mathbb{B}_k^{\mathrm{curl}} = \mathbf{d}\mathbb{B}_k^{\mathrm{div}} = \mathbf{d}\mathbb{P}_k$, and

$$\mathbb{C}_k = \mathrm{d}\mathbb{P}_{k-1}(\mathcal{C}) \times \mathrm{d}\mathbb{P}_k(\mathcal{S}).$$

3. **Optimal approximation spaces on quadrangles.** The case of quadrangular meshes is quite surprising because the lowest order approximation space (namely with $\mathbb{A}_{k+1} = \mathbb{Q}_1$) does not give the classical finite volume vector space, but rather an enriched version including three basis vector instead of two:

$$\mathbf{d}\mathbb{B}_0^{\mathrm{div}} = \mathrm{Span}\left(\begin{pmatrix} 1 \\ 0 \end{pmatrix}, \begin{pmatrix} 0 \\ 1 \end{pmatrix}, \begin{pmatrix} -x \\ y \end{pmatrix}\right),$$

and

$$\mathbf{d}\mathbb{B}_0^{\mathrm{curl}} = \mathrm{Span}\left(\begin{pmatrix} 1 \\ 0 \end{pmatrix}, \begin{pmatrix} 0 \\ 1 \end{pmatrix}, \begin{pmatrix} y \\ x \end{pmatrix}\right).$$

In the general case, we denote by $\mathrm{d}\mathbb{Q}_{i,j}$ the space of polynomials of degree lower than i in x and lower than j in y, and we set

$$\mathbf{d}\mathbb{B}_k^{\mathrm{div}} = [(\mathrm{d}\mathbb{Q}_{k,k} + \mathrm{d}\mathbb{Q}_{k+1,k-1}) \times (\mathrm{d}\mathbb{Q}_{k,k} + \mathrm{d}\mathbb{Q}_{k-1,k+1})] \oplus \mathrm{Span}\begin{pmatrix} -x^{k+1}y^k \\ x^k y^{k+1} \end{pmatrix}$$

and

$$\mathbf{d}\mathbb{B}_k^{\mathrm{curl}} = [(\mathrm{d}\mathbb{Q}_{k,k} + \mathrm{d}\mathbb{Q}_{k-1,k+1}) \times (\mathrm{d}\mathbb{Q}_{k,k} + \mathrm{d}\mathbb{Q}_{k+1,k-1})] \oplus \mathrm{Span}\begin{pmatrix} x^k y^{k+1} \\ x^{k+1}y^k \end{pmatrix}.$$

Last, the space $\mathbb{C}_k$ is

$$\mathbb{C}_k = \mathrm{d}\breve{\mathbb{Q}}_k(\mathcal{C}) \times \mathrm{d}\mathbb{P}_{k-1}(\mathcal{S}),$$

with

$$\mathrm{d}\breve{\mathbb{Q}}_k := \mathrm{d}\mathbb{Q}_{k,k-1} + \mathrm{d}\mathbb{Q}_{k-1,k},$$

or more clearly, $\mathrm{d}\breve{\mathbb{Q}}_k$ contains all canonical monomials of $\mathrm{d}\mathbb{Q}_k$ except for $x^k y^k$. As remarked in [54], the difference with the discontinuous Nédélec and Raviart-Thomas elements is, in this case, only of a single element, and the benefits of this optimal basis with respect to the classical one is less evident.

The scalar product on the finite element spaces will be denoted with $\langle \cdot | \cdot \rangle$ with the finite element space as index, e.g. $\langle \cdot | \cdot \rangle_{\mathbb{A}_{k+1}}$. When the space of differential forms will be needed, we will take the same notation, but with gothic letters, e.g. $\langle \cdot | \cdot \rangle_{\mathfrak{A}_{k+1}}$ is the scalar product on the discrete space of differential forms which proxies are in $\mathbb{A}_{k+1}$.

Last, as the space $\mathbb{C}_k$ includes in general both components in the cell and components in the face, the scalar product in $\mathbb{C}_k$ is the graph scalar product:

$$\langle f | g \rangle_{\mathbb{C}_k} := \sum_{c \in \mathcal{C}} \int_c f^C g^C + \sum_{S \in \mathcal{S}} \int_S f^S g^S.$$

3 Discrete Hodge-star operator, codifferentials and Hodge Laplacian

3.1 Discrete Hodge star operator

Our discrete de-Rham complex includes the 0, 1 and 2-forms. For completing the discrete counterpart of the continuous de-Rham complex, we wish to define the discrete Hodge-star operators, which we denote by $\bigstar_{\{k\}}$ for the Hodge-star operator mapping the k forms to the $d-k$ forms. In dimension 2, the Hodge star operator $\bigstar_{\{1\}}$ maps the 1-forms to themselves, and is translated in terms of proxy as a $\pi/2$ rotation. We define the discrete operator $\bigstar_{\{1\}}$ also as a $\pi/2$ rotation.

We now define the discrete Hodge star operators $\bigstar_{\{0\}}$ and $\bigstar_{\{2\}}$ between the discrete spaces $\mathbb{A}_{k+1}$ and $\mathbb{C}_k$. If the approximation degrees are considered, we see that the space $\mathbb{A}_{k+1}$ is of a higher degree per cell and per side, which means that a projection should be a good option for the definition of the Hodge star operator $\bigstar_{\{0\}}$:

Definition 2 (Definition of $\bigstar_{\{0\}}$)**.** *The Hodge star operator $\bigstar_{\{0\}}$ that maps $\mathbb{A}_{k+1}$ to $\mathbb{C}_k$ is defined as*

$$\begin{array}{rccl} \bigstar_{\{0\}}: & \mathbb{A}_{k+1} & \longmapsto & \mathbb{C}_k \\ & \varphi & \longmapsto & \bigstar_{\{0\}}(\varphi) := \left\{ \begin{array}{ll} \mathcal{P}_C(\varphi) & \forall C \in \mathcal{C} \\ \mathcal{P}_S(\varphi) & \forall S \in \mathcal{S} \end{array} \right. \end{array} \tag{6}$$

where $\mathcal{P}$ is the L^2 projection.

We now define the discrete Hodge star operator $\bigstar_{\{2\}}$. For a given $\Psi \in \mathbb{C}_k$, we wish to define $\bigstar_{\{2\}}$ such that

$$\forall \varphi \in \mathbb{A}_{k+1} \qquad \left\langle \bigstar_{\{2\}}(\Psi) \, | \varphi \right\rangle_{\mathbb{A}_{k+1}} = \left\langle \Psi | \bigstar_{\{0\}} \varphi \right\rangle_{\mathbb{C}_k}$$

This can be developed on one hand as

$$\left\langle \bigstar_{\{2\}}(\Psi) \, | \varphi \right\rangle_{\mathbb{A}_{k+1}} = \sum_{C \in \mathcal{C}} \int_C \bigstar_{\{2\}}(\Psi) \, \varphi,$$

and on the other hand as

$$\left\langle \Psi | \bigstar_{\{0\}} \varphi \right\rangle_{\mathbb{C}_k} = \sum_{C \in \mathcal{C}} \int_C \Psi \bigstar_{\{0\}}(\varphi) + \sum_{S \in \mathcal{S}} \int_S \Psi \bigstar_{\{0\}}(\varphi).$$

By definition of the projection, this may be simplified as

$$\left\langle \Psi | \bigstar_{\{0\}}(\varphi) \right\rangle_{\mathbb{C}_k} = \sum_{C \in \mathcal{C}} \int_C \Psi^C \varphi + \sum_{S \in \mathcal{S}} \int_S \Psi^S \varphi,$$

and this leads to the following definition:

Definition 3 (Definition of $\bigstar_{\{2\}}$)**.** *The Hodge star operator $\bigstar_{\{2\}}$ that maps $\mathbb{C}_k$ to $\mathbb{A}_{k+1}$ is defined as*

$$\forall \varphi \in \mathbb{A}_{k+1} \quad \forall \psi \in \mathbb{C}_k \qquad \sum_{C \in \mathcal{C}} \int_C \bigstar_{\{2\}}(\psi) \varphi = \sum_{C \in \mathcal{C}} \int_C \psi^C \varphi + \sum_{S \in \mathcal{S}} \int_S \psi^S \varphi.$$

Note that the computation of $\bigstar_{\{2\}}$ as in Definition 3 requires the inversion of the mass matrix of $\mathbb{A}_{k+1}$.

Remark 1. Following [54], we always have

$$\dim \mathbb{C}_k > \dim \mathbb{A}_{k+1},$$

which means that neither $\bigstar_{\{0\}}$ nor $\bigstar_{\{2\}}$ can be invertible.

Also, following the rank nullity theorem, we have

$$\dim \left(\ker \bigstar_{\{2\}} \right) = \dim \mathbb{C}_k - \operatorname{rank} \left(\bigstar_{\{2\}} \right) \geq \dim \mathbb{C}_k - \dim \mathbb{A}_{k+1} > 0,$$

which means that $\bigstar_{\{2\}}$ has always a non trivial kernel.

It is however easy to check that $\bigstar_{\{2\}} \circ \bigstar_{\{0\}} = \mathrm{I}_d$.

3.2 Definition of the codifferential operators

3.2.1 Definition of δ^1

The continuous codifferential δ^1 was defined in (3). We wish to find a formula for the discrete codifferential on the proxies. We focus on the proxy choice (2).

Proposition 1 (Definition of $\left(\nabla^\perp\right)^\star$)**.** *$\left(\nabla^\perp\right)^\star$ is defined as in (3) but with the discrete operators. It ensures*

$$\forall \mathbf{u} \in \mathbf{d}\mathbb{B}_k^{\mathrm{div}} \quad \forall f \in \mathbb{A}_{k+1} \qquad \left\langle \left(\nabla^\perp\right)^\star \mathbf{u} | f \right\rangle_{\mathbb{A}_{k+1}} = \left\langle \mathbf{u} | \nabla^\perp f \right\rangle_{\mathbf{d}\mathbb{B}_k^{\mathrm{div}}}.$$

Proof. The composition of d^1 with $\bigstar_{\{1\}}$ appearing in (3) is a $\left(\nabla^\perp \cdot\right)$ on the proxy, which is translated into a $\left(\nabla^\perp_{\mathscr{D}'} \cdot\right)$ at a discrete level. Then for $\mathbf{u} \in \mathbf{d}\mathbb{B}_k^{\mathrm{div}}$,

$$\mathrm{Proxy}\left(\mathrm{d}^1 \bigstar_{\{1\}} \mathfrak{u}\right) = \begin{cases} \forall C \in \mathcal{C} & \nabla^\perp \cdot \mathbf{u} \\ \forall S \in \mathcal{S} & \left[\!\left[\mathbf{u}^\perp \cdot \mathbf{n}\right]\!\right] \end{cases}$$

Then

$$\begin{aligned}
\left\langle \left(\nabla^\perp\right)^\star \mathbf{u} | f \right\rangle_{\mathbb{A}_{k+1}} &= \left\langle \bigstar_{\{2\}} \mathrm{d}^1 \bigstar_{\{1\}} \mathfrak{u} | \mathfrak{f} \right\rangle_{\mathbb{A}_{k+1}} \\
&= \left\langle \bigstar_{\{2\}} \mathrm{Proxy}\left(\mathrm{d}^1 \bigstar_{\{1\}} \mathfrak{u}\right) | f \right\rangle_{\mathbb{A}_{k+1}} \\
&= \sum_{C \in \mathcal{C}} \int_C f \nabla^\perp \cdot \mathbf{u} + \sum_{S \in \mathcal{S}} \int_S \left[\!\left[\mathbf{u}^\perp \cdot \mathbf{n}\right]\!\right] f \\
&= -\sum_{C \in \mathcal{C}} \int_C f \nabla \cdot \mathbf{u}^\perp + \sum_{S \in \mathcal{S}} \int_S \left[\!\left[\mathbf{u}^\perp \cdot \mathbf{n}\right]\!\right] f \\
&= -\sum_{C \in \mathcal{C}} \int_C \nabla \cdot \left(f \mathbf{u}^\perp\right) - \sum_{C \in \mathcal{C}} \int_C \mathbf{u}^\perp \cdot \nabla f + \sum_{S \in \mathcal{S}} \int_S \left[\!\left[\mathbf{u}^\perp \cdot \mathbf{n}\right]\!\right] f \\
&= -\sum_{S \in \mathcal{S}} \int_S f \left[\!\left[\mathbf{u}^\perp \cdot \mathbf{n}\right]\!\right] - \sum_{C \in \mathcal{C}} \int_C \mathbf{u}^\perp \cdot \nabla f + \sum_{S \in \mathcal{S}} \int_S \left[\!\left[\mathbf{u}^\perp \cdot \mathbf{n}\right]\!\right] f \\
&= -\sum_{C \in \mathcal{C}} \int_C \mathbf{u}^\perp \cdot \nabla f \\
&= \sum_{C \in \mathcal{C}} \int_C \mathbf{u} \cdot \nabla^\perp f \\
\left\langle \left(\nabla^\perp\right)^\star \mathbf{u} | f \right\rangle_{\mathbb{A}_{k+1}} &= \left\langle \mathbf{u} | \nabla^\perp f \right\rangle_{\mathbf{d}\mathbb{B}_k^{\mathrm{div}}},
\end{aligned}$$

which ends the proof. □

3.2.2 Definition of δ^2

The continuous codifferential δ^2 was defined in (4). Still, δ^2 depends on $\bigstar_{\{2\}}$, and as stated in Remark 1, $\bigstar_{\{2\}}$ has a non trivial kernel, which may lead to a mismatch between the properties of the discrete and continuous codifferentials. This is why we define the discrete codifferential δ^2 as follows

Definition 4 (Definition of $(-\nabla_{\mathscr{D}'} \cdot)^\star$)**.** *$(-\nabla_{\mathscr{D}'} \cdot)^\star$ is defined as*

$$\forall \mathbf{u} \in \mathbf{d}\mathbb{B}_k^{\mathrm{div}} \quad \forall f \in C_k \qquad \left\langle (-\nabla_{\mathscr{D}'} \cdot)^\star f | \mathbf{u} \right\rangle_{\mathbf{d}\mathbb{B}_k^{\mathrm{div}}} = \left\langle f | -\nabla_{\mathscr{D}'} \cdot \mathbf{u} \right\rangle_{\mathbb{C}_k}.$$

We however still have an identity similar to (4) at the discrete level

Proposition 2. *If the discrete proxy of δ^2 is defined as in Definition 4, then*

$$\delta^2 \circ \bigstar_{\{0\}} = -\bigstar_{\{1\}} \circ \mathrm{d}^0.$$

Proof. We denote by $\mathfrak{f} \in \mathbb{A}_{k+1}$ and and $\mathfrak{u} \in \mathfrak{B}_k$. Then

$$\begin{aligned}
\left\langle \delta^2 \circ \bigstar_{\{0\}} \mathfrak{f} | \mathfrak{u} \right\rangle_{\mathfrak{B}_k} &= \left\langle (-\nabla_{\mathscr{D}'} \cdot)^\star \bigstar_{\{0\}} f | \mathbf{u} \right\rangle_{\mathbf{dB}_k^{\mathrm{div}}} \\
&= -\left\langle \bigstar_{\{0\}} f | \nabla_{\mathscr{D}'} \cdot \mathbf{u} \right\rangle_{\mathbb{C}_k} \\
&= -\sum_{c \in \mathcal{C}} \int_C f \nabla \cdot \mathbf{u} + \sum_{S \in \mathcal{S}} \int_S f \left[\!\left[\mathbf{u} \cdot \mathbf{n} \right]\!\right] \\
&= -\sum_{c \in \mathcal{C}} \int_C \nabla \cdot (f \mathbf{u}) + \sum_{c \in \mathcal{C}} \int_C \mathbf{u} \cdot \nabla f + \sum_{S \in \mathcal{S}} \int_S f \left[\!\left[\mathbf{u} \cdot \mathbf{n} \right]\!\right] \\
&= \sum_{c \in \mathcal{C}} \int_C \mathbf{u} \cdot \nabla f \\
&= -\sum_{c \in \mathcal{C}} \int_C \mathbf{u} \cdot \left(\nabla^\perp f \right)^\perp \\
\left\langle \delta^2 \circ \bigstar_{\{0\}} \mathfrak{f} | \mathfrak{u} \right\rangle_{\mathfrak{B}_k} &= -\left\langle \bigstar_{\{1\}} \circ \mathrm{d}^0 \mathfrak{f} | \mathfrak{u} \right\rangle_{\mathfrak{B}_k},
\end{aligned}$$

which ends the proof. □

3.3 Hodge Laplacian

Even if we are dealing with hyperbolic systems, the Laplace operator plays a role as a regularization operator, this is why a small section is dedicated to this operator. The Hodge-Laplacian is defined as $\delta^{i+1} \circ \mathrm{d}^i + \mathrm{d}^{i-1} \circ \delta^i$. We are interested in this operator only on $\mathfrak{B}_k$. As we are dealing with Galerkin methods, we are rather interested in the L^2 product of the Hodge Laplacian of a $\mathfrak{u} \in \mathfrak{B}_k$ with a given $\mathfrak{v} \in \mathfrak{B}_k$.

Proposition 3 (Expression of $\delta^2 \circ \mathrm{d}^1$)**.** *For (1) as a choice of proxy, for all* $\mathfrak{u}, \mathfrak{v} \in \mathfrak{B}_k$

$$\begin{aligned}
\left\langle \delta^2 \circ \mathrm{d}^1 \mathfrak{u} | \mathfrak{v} \right\rangle_{\mathfrak{B}_k} &= \left\langle \left(\nabla^\perp \cdot \right)^\star \nabla^\perp \cdot \mathbf{u} | \mathbf{v} \right\rangle_{\mathbf{dB}_k^{\mathrm{curl}}} \\
&= \sum_{c \in \mathcal{C}} \int_c \left(\nabla^\perp \cdot \mathbf{u} \right) \left(\nabla^\perp \cdot \mathbf{v} \right) + \sum_{S \in \mathcal{S}} \int_S \left[\!\left[\mathbf{u} \right]\!\right]^T \left(\mathrm{I}_2 - \mathbf{n}^T \mathbf{n} \right) \left[\!\left[\mathbf{v} \right]\!\right].
\end{aligned} \tag{7}$$

For (2) as a choice of proxy, for all $\mathfrak{u}, \mathfrak{v} \in \mathfrak{B}_k$

$$\begin{aligned}
\left\langle \delta^2 \circ \mathrm{d}^1 \mathfrak{u} | \mathfrak{v} \right\rangle_{\mathfrak{B}_k} &= \left\langle (\nabla \cdot)^\star \nabla \cdot \mathbf{u} | \mathbf{v} \right\rangle_{\mathbf{dB}_k^{\mathrm{curl}}} \\
&= \sum_{c \in \mathcal{C}} \int_c \left(\nabla \cdot \mathbf{u} \right) \left(\nabla \cdot \mathbf{v} \right) + \sum_{S \in \mathcal{S}} \int_S \left[\!\left[\mathbf{u} \right]\!\right]^T \left(\mathbf{n}^T \mathbf{n} \right) \left[\!\left[\mathbf{v} \right]\!\right].
\end{aligned} \tag{8}$$

Proof. We first deal with the choice (1) of proxies:

$$\begin{aligned}
\left\langle \delta^2 \circ \mathrm{d}^1 \mathfrak{u} | \mathfrak{v} \right\rangle_{\mathfrak{B}_k} &= \left\langle \left(\nabla^\perp \cdot \right)^\star \nabla^\perp \cdot \mathbf{u} | \mathbf{v} \right\rangle_{\mathbf{dB}_k^{\mathrm{curl}}} \\
&= \left\langle \nabla^\perp \cdot \mathbf{u} | \nabla^\perp \cdot \mathbf{v} \right\rangle_{\mathbf{dB}_k^{\mathrm{curl}}} \\
&= \sum_{c \in \mathcal{C}} \int_c \left(\nabla^\perp \cdot \mathbf{u} \right) \left(\nabla^\perp \cdot \mathbf{v} \right) + \sum_{S \in \mathcal{S}} \int_S \left[\!\left[\mathbf{u} \cdot \mathbf{n}^\perp \right]\!\right] \left[\!\left[\mathbf{v} \cdot \mathbf{n}^\perp \right]\!\right] \\
\left\langle \delta^2 \circ \mathrm{d}^1 \mathfrak{u} | \mathfrak{v} \right\rangle_{\mathfrak{B}_k} &= \sum_{c \in \mathcal{C}} \int_c \left(\nabla^\perp \cdot \mathbf{u} \right) \left(\nabla^\perp \cdot \mathbf{v} \right) + \sum_{S \in \mathcal{S}} \int_S \left[\!\left[\mathbf{u} \right]\!\right]^T \mathbf{n}^\perp \left(\mathbf{n}^\perp \right)^T \left[\!\left[\mathbf{v} \right]\!\right],
\end{aligned}$$

and we have

$$\mathbf{n}^\perp \left(\mathbf{n}^\perp \right)^T = \begin{pmatrix} -\mathbf{n}_y \\ \mathbf{n}_x \end{pmatrix} \begin{pmatrix} -\mathbf{n}_y & \mathbf{n}_x \end{pmatrix} = \begin{pmatrix} \mathbf{n}_y^2 & -\mathbf{n}_x \mathbf{n}_y \\ -\mathbf{n}_x \mathbf{n}_y & \mathbf{n}_x^2 \end{pmatrix} = \mathrm{I}_2 - \mathbf{n}^T \mathbf{n},$$

which finally gives (7). (8) may be obtained in the same manner. □

The case of $\mathrm{d}^0 \circ \delta^1$ is harder to address, because of the computation of δ^1. As it maps to $\mathbb{A}_{k+1}$, its computation requires the inversion of the mass matrix of $\mathbb{A}_{k+1}$ which is a continuous finite element space and so is not local. It is probably possible to simplify it by using mass lumping, still for the remaining of the article, only the expression of $\delta^2 \circ \mathrm{d}^1$ matters. This is why the case of $\mathrm{d}^0 \circ \delta^1$ is not further investigated.

4 Discrete preservation of the curl or the divergence

4.1 Numerical scheme

In this section, we consider a system of conservation law in which one of the unknowns is a vector $\mathbf{u}$. We denote by $\overline{\mathbf{G}}$ the flux of the conservation law involving $\mathbf{u}$

$$\partial_t \mathbf{u} + \boldsymbol{\nabla} \cdot \overline{\mathbf{G}} = 0. \tag{9}$$

We consider the numerical resolution of (9) on a periodic domain. The discontinuous Galerkin method reads

$$\text{Find } \mathbf{u} \in \mathbb{B} \quad \forall \mathbf{v} \in \mathbb{B} \qquad \sum_{C \in \mathcal{C}} \int_C \mathbf{v} \cdot \partial_t \mathbf{u} - \sum_{C \in \mathcal{C}} \int_C \overline{\mathbf{G}} : \boldsymbol{\nabla} \mathbf{v} + \sum_{S \in \mathcal{S}} \int_S [\![\mathbf{v}]\!] \cdot \widetilde{\mathbf{G}} = 0, \tag{10}$$

where $\widetilde{\mathbf{G}}$ is the numerical flux, and $\mathbb{B}$ is the approximation space for vectors that is not defined for the moment.

4.2 Discrete preservation of the vorticity

In this section, we consider the case in which $\overline{\mathbf{G}}$ is proportional to the identity $\overline{\mathbf{G}} = g \mathrm{I}_d$, which means that we have $\boldsymbol{\nabla} \cdot \overline{\mathbf{G}} = \nabla g$. This means that the conservation law on $\mathbf{u}$ (9) may be simplified as

$$\partial_t \mathbf{u} + \nabla g = 0, \tag{11}$$

where g is a scalar that may depend nonlinearly on the variables of the system. Then the discontinuous Galerkin discretization reads

$$\text{Find } \mathbf{u} \in \mathbf{d}\mathbb{B}_k^{\mathrm{div}} \quad \forall \mathbf{v} \in \mathbf{d}\mathbb{B}_k^{\mathrm{div}} \qquad \sum_{C \in \mathcal{C}} \int_C \mathbf{v} \cdot \partial_t \mathbf{u} - \sum_{C \in \mathcal{C}} \int_C g \nabla \cdot \mathbf{v} + \sum_{S \in \mathcal{S}} \int_S [\![\mathbf{v}]\!] \cdot \widetilde{\mathbf{G}} = 0, \tag{12}$$

where $\widetilde{\mathbf{G}}$ is the numerical flux. Equation (11) induces formally the conservation of $\nabla^\perp \cdot \mathbf{u}$, and the discontinuous Galerkin method (12) may have a similar property summarized in the following proposition.

Proposition 4 (Conservation of $\left(\nabla^\perp \mathbf{u}\right)^\star$)**.** *Consider the numerical scheme* (12)*. If* $\widetilde{\mathbf{G}}$ *is parallel to* $\mathbf{n}$*, then the numerical scheme* (12) *induces* $\partial_t \left(\left(\nabla^\perp\right)^\star \mathbf{u} \right) = 0$*.*

Proof. If $\widetilde{\mathbf{G}}$ is parallel to $\mathbf{n}$, then the numerical flux may be rewritten

$$\widetilde{\mathbf{G}} = \tilde{g} \mathbf{n},$$

where $\tilde{g}$ is a scalar, so that the numerical scheme (12) may be rewritten

$$\text{Find } \mathbf{u} \quad \forall \mathbf{v} \qquad \sum_{C \in \mathcal{C}} \int_C \mathbf{v} \cdot \partial_t \mathbf{u} - \sum_{C \in \mathcal{C}} \int_C g \nabla \cdot \mathbf{v} + \sum_{S \in \mathcal{S}} \int_S [\![\mathbf{v} \cdot \mathbf{n}]\!] \, \tilde{g} = 0.$$

In this last equation, suppose that $\mathbf{v} = \nabla^\perp f$ for $f \in \mathbb{A}_{k+1}$. Then the normal jump vanishes at each side:

$$\forall S \in \mathcal{S} \qquad [\![\mathbf{v} \cdot \mathbf{n}]\!] = 0,$$

and on each cell, its strong divergence is 0:

$$\nabla \cdot \mathbf{v} = 0,$$

so that

$$\forall f \in \mathbb{A}_{k+1} \qquad \sum_{C \in \mathcal{C}} \int_C \left(\nabla^\perp f\right) \cdot \partial_t \mathbf{u} = 0.$$

This last equation means that

$$\forall f \in \mathbb{A}_{k+1} \qquad \left\langle \nabla^\perp f | \partial_t \mathbf{u} \right\rangle_{\mathbf{d}\mathbb{B}_k^{\mathrm{div}}} = 0.$$

By definition of $\left(\nabla^\perp\right)^\star$, we get

$$\forall f \in \mathbb{A}_{k+1} \qquad \left\langle f | \left(\nabla^\perp\right)^\star (\partial_t \mathbf{u}) \right\rangle_{\mathbf{d}\mathbb{B}_k^{\mathrm{div}}} = 0.$$

It remains to prove that $\left(\nabla^\perp\right)^\star (\partial_t \mathbf{u}) = \partial_t \left(\left(\nabla^\perp\right)^\star \mathbf{u} \right)$. Denoting by f an element of $\mathbb{A}_{k+1}$, we have

$$\begin{aligned}
\left\langle \partial_t \left(\left(\nabla^\perp\right)^\star \mathbf{u} \right) | f \right\rangle_{\mathbb{A}_{k+1}} &= \int_\Omega \partial_t \left(\left(\nabla^\perp\right)^\star \mathbf{u} \right) f \\
&= \partial_t \left(\int_\Omega \left(\left(\nabla^\perp\right)^\star \mathbf{u} \right) f \right) \\
&= \partial_t \left(\int_\Omega \mathbf{u} \cdot \nabla^\perp f \right) \\
&= \int_\Omega (\partial_t \mathbf{u}) \cdot \nabla^\perp f \\
&= \left\langle \partial_t \mathbf{u} | \nabla^\perp f \right\rangle_{\mathbf{d}\mathbb{B}_k^{\mathrm{div}}} \\
\left\langle \partial_t \left(\left(\nabla^\perp\right)^\star \mathbf{u} \right) | f \right\rangle_{\mathbb{A}_{k+1}} &= \left\langle \left(\nabla^\perp\right)^\star (\partial_t \mathbf{u}) | f \right\rangle_{\mathbb{A}_{k+1}},
\end{aligned}$$

which ends the proof. □

Remark 2. The Proposition 4 was proven in the semi-discrete case. It is however easy to prove the same in the discrete case. Still, the definition of the adjoint curl $\left(\nabla^\perp\right)^\star$ should take into account how the mass matrix is computed. For example, if the mass matrix is lumped, then the adjoint curl should be defined with the same lumped mass matrix.

Remark 3 (Lax-Friedrich flux with normal diffusion)**.** A widely used numerical flux is the Lax-Friedrich flux which reads

$$\widetilde{\mathbf{G}}\left(\overline{\mathbf{G}}_L, \mathbf{u}_L, \overline{\mathbf{G}}_R, \mathbf{u}_R, \mathbf{n}\right) = \frac{\overline{\mathbf{G}}_L \mathbf{n} + \overline{\mathbf{G}}_R \mathbf{n}}{2} + \frac{\lambda}{2}\left(\mathbf{u}_L - \mathbf{u}_R\right), \tag{13}$$

where λ is the maximum absolute value of the eigenvalues of the system. Dealing with the system (11), the numerical flux (13) can be simplified as

$$\widetilde{\mathbf{G}}\left(g_L, \mathbf{u}_L, g_R, \mathbf{u}_R, \mathbf{n}\right) = \frac{g_L \mathbf{n} + g_R \mathbf{n}}{2} + \frac{\lambda}{2}\left(\mathbf{u}_L - \mathbf{u}_R\right).$$

The centered part of the flux is clearly parallel to the normal, and should not be modified because it ensures the consistency of the numerical scheme. The diffusive part may be decomposed into its normal and tangential part as

$$\left(\mathbf{u}_L - \mathbf{u}_R\right) = \mathbf{n}\mathbf{n}^T\left(\mathbf{u}_L - \mathbf{u}_R\right) + \left(\mathrm{I}_d - \mathbf{n}\mathbf{n}^T\right)\left(\mathbf{u}_L - \mathbf{u}_R\right).$$

Therefore an easy way to ensure the hypothesis of Proposition 4 is to use the following *Lax-Friedrich flux with purely normal diffusion*

$$\widetilde{\mathbf{G}}\left(g_L, \mathbf{u}_L, g_R, \mathbf{u}_R, \mathbf{n}\right) = \frac{g_L \mathbf{n} + g_R \mathbf{n}}{2} + \frac{\lambda \mathbf{n}\mathbf{n}^T}{2}\left(\mathbf{u}_L - \mathbf{u}_R\right). \tag{14}$$

Remark 4 (Link with the Hodge Laplacian)**.** The diffusion induced by (14) is exactly the face component of the component $\delta^2 \circ \mathrm{d}^1$ of the Hodge Laplacian that was found in (8). Formally, the numerical resolution of (11) with the numerical flux (14) may then be seen as

$$\partial_t \mathfrak{u} - \delta^2 \tilde{\mathfrak{f}} = \lambda \widetilde{\delta^2 \circ \mathrm{d}^1} \mathfrak{u},$$

where $\widetilde{\delta^2 \circ \mathrm{d}^1}$ is the face component of the operator $\delta^2 \circ \mathrm{d}^1$, and $\tilde{\mathfrak{f}}$ is the projection of $\mathfrak{f}$ on the space $\mathbb{C}_k$. The conservation of the adjoint curl is then translated into $\partial_t\left(\delta^1 \mathfrak{u}\right) = 0$.

4.3 Discrete preservation of the irrotational component

In this section, we consider the case in which $\overline{\mathbf{G}}$ is antisymmetric; in dimension 2, $\overline{\mathbf{G}}$ may be written as

$$\begin{pmatrix} 0 & -g \\ g & 0 \end{pmatrix},$$

where g is a scalar that may depend nonlinearly on the variables of the system. This means that $\mathbf{u}$ ensures the following conservation law

$$\partial_t \mathbf{u} + \nabla^\perp g = 0. \tag{15}$$

Then the discontinuous Galerkin discretization reads

$$\text{Find } \mathbf{u} \in \mathbf{d}\mathbb{B}_k^{\text{curl}} \quad \forall \mathbf{v} \in \mathbf{d}\mathbb{B}_k^{\text{curl}} \qquad \sum_{C\in\mathcal{C}} \int_C \mathbf{v}\cdot\partial_t\mathbf{u} - \sum_{C\in\mathcal{C}} \int_C g\nabla^\perp\cdot\mathbf{v} + \sum_{S\in\mathcal{S}} \int_S [\![\mathbf{v}]\!]\cdot\widetilde{\mathbf{G}} = 0, \tag{16}$$

where $\widetilde{\mathbf{G}}$ is the numerical flux.

Proposition 5 (Adjoint conservation of the divergence)**.** *Consider the numerical scheme* (16)*. If* $\widetilde{\mathbf{G}}$ *is orthogonal to* $\mathbf{n}$*, then* $(\nabla)^\star\mathbf{u}$ *is conserved by the numerical scheme.*

The proof of Proposition 5 follows exactly the same lines as Proposition 4 and is not repeated.

Remark 5 (Lax-Friedrich flux with purely tangential diffusion)**.** The Lax-Friedrich numerical flux (13) for (15) may be simplified as

$$\widetilde{\mathbf{G}}\left(\mathbf{g}_L,\mathbf{u}_L,\mathbf{g}_R,\mathbf{u}_R,\mathbf{n}\right) = \frac{g_L\mathbf{n}^\perp + g_R\mathbf{n}^\perp}{2} + \frac{\lambda}{2}\left(\mathbf{u}_L - \mathbf{u}_R\right).$$

The centered part of the flux, which is clearly orthogonal to $\mathbf{n}$, ensures the consistency of the numerical scheme. Still relying on the decomposition of the diffusive part into its normal and tangential part, an easy way to ensure the hypothesis of Proposition 5 consists in using the following *Lax-Friedrich flux with purely tangential diffusion*

$$\widetilde{\mathbf{G}}\left(\mathbf{g}_L,\mathbf{u}_L,\mathbf{g}_R,\mathbf{u}_R,\mathbf{n}\right) = \frac{g_L\mathbf{n}^\perp + g_R\mathbf{n}^\perp}{2} + \frac{\lambda\left(\mathrm{I}_d - \mathbf{n}\mathbf{n}^T\right)}{2}\left(\mathbf{u}_L - \mathbf{u}_R\right). \tag{17}$$

The diffusion of (17) matches with the face component of the $\delta^2\circ\mathrm{d}^1$ component of the Hodge Laplacian (7).

Last, we remark by translating back the equation into differential forms, the same equation as in Remark 4 holds.

5 Preservation of initially curl or divergence free fields for Lie derivative based advection equation

5.1 The direct and adjoint continuous equations

In this section, we address a slightly different problem, in which a vector field is seen as a proxy of the advection equation based on the *Lie derivative*. We first introduce an operator on the differential forms Λ^k for $k \geq 1$ the *contraction by a vector* $\mathbf{b}$. It is defined as

$$\begin{array}{rccc} i_{\mathbf{b}} & : & \Lambda^k & \longmapsto & \Lambda^{k-1} \\ & & \mathfrak{u} & \longmapsto & i_{\mathbf{b}}\mathfrak{u}, \end{array}$$

with

$$\forall \mathbf{v}_1,\dots\mathbf{v}_{k-1}\in\mathbb{R}^2 \qquad i_{\mathbf{b}}\mathfrak{u}\left(\mathbf{v}_1,\dots\mathbf{v}_{k-1}\right) := \mathfrak{u}\left(\mathbf{b},\mathbf{v}_1,\dots\mathbf{v}_{k-1}\right).$$

We also define the *co-contraction* $j_{\mathbf{b}}$ as

$$\begin{array}{rccc} j_{\mathbf{b}} & : & \Lambda^k & \longmapsto & \Lambda^{k+1} \\ & & \mathfrak{u} & \longmapsto & j_{\mathbf{b}}\mathfrak{u}, \end{array}$$

such that $\bigstar_{\{k+1\}} \circ j_{\mathbf{b}} = (-1)^k i_{\mathbf{b}} \circ \bigstar_{\{k\}}$.

- If the choice (1) is done, then

$$\left\{ \begin{array}{llll} \forall \mathfrak{f} \in \Lambda^2 & \mathrm{Proxy}(\mathfrak{f}) = f & & \mathrm{Proxy}\left(i_{\mathbf{b}}\mathfrak{f}\right) = f\mathbf{b}^\perp \\ \forall \mathfrak{u} \in \Lambda^1 & \mathrm{Proxy}(\mathfrak{u}) = \mathbf{u} & & \mathrm{Proxy}\left(i_{\mathbf{b}}\mathfrak{u}\right) = \mathbf{u} \cdot \mathbf{b}, \\ \forall \mathfrak{f} \in \Lambda^0 & \mathrm{Proxy}(\mathfrak{f}) = f & & \mathrm{Proxy}\left(j_{\mathbf{b}}\mathfrak{f}\right) = f\mathbf{b}, \\ \forall \mathfrak{u} \in \Lambda^1 & \mathrm{Proxy}(\mathfrak{u}) = \mathbf{u} & & \mathrm{Proxy}\left(j_{\mathbf{b}}\mathfrak{u}\right) = -\mathbf{u}^\perp \cdot \mathbf{b}, \end{array} \right.$$

- If the choice (2) is done, then

$$\left\{ \begin{array}{llll} \forall \mathfrak{f} \in \Lambda^2 & \mathrm{Proxy}^\perp(\mathfrak{f}) = f & & \mathrm{Proxy}^\perp\left(i_{\mathbf{b}}\mathfrak{f}\right) = -f\mathbf{b} \\ \forall \mathfrak{u} \in \Lambda^1 & \mathrm{Proxy}^\perp(\mathfrak{u}) = \mathbf{u} & & \mathrm{Proxy}^\perp\left(i_{\mathbf{b}}\mathfrak{u}\right) = \det\left(\mathbf{b}, \mathbf{u}\right) \\ \forall \mathfrak{f} \in \Lambda^0 & \mathrm{Proxy}^\perp(\mathfrak{f}) = f & & \mathrm{Proxy}^\perp\left(j_{\mathbf{b}}\mathfrak{f}\right) = f\mathbf{b}^\perp, \\ \forall \mathfrak{u} \in \Lambda^1 & \mathrm{Proxy}^\perp(\mathfrak{u}) = \mathbf{u} & & \mathrm{Proxy}^\perp\left(j_{\mathbf{b}}\mathfrak{u}\right) = -\mathbf{u} \cdot \mathbf{b}, \end{array} \right.$$

The *Lie derivative* $\mathrm{L}_{\mathbf{b}}$ is defined as

$$\begin{array}{rccc} \mathrm{L}_{\mathbf{b}} & : & C^\infty\Lambda^k & \longmapsto & C^\infty\Lambda^k \\ & & \mathfrak{u} & \longmapsto & \mathrm{L}_{\mathbf{b}}\,\mathfrak{u} = i_{\mathbf{b}} \circ \mathrm{d}^k\mathfrak{u} + \mathrm{d}^{k-1} \circ i_{\mathbf{b}}\mathfrak{u}. \end{array}$$

We consider the following advection equation discussed in [36, 38, 37, 53]

$$\partial_t \mathfrak{u} + \mathrm{L}_{\mathbf{b}}\,\mathfrak{u} = 0. \tag{18}$$

It is easy to check that the Lie derivative commutes with the exterior derivative, so that if $\mathfrak{u}$ follows (18), then

$$\partial_t\left(\mathrm{d}^k\mathfrak{u}\right) + \mathrm{L}_{\mathbf{b}}\left(\mathrm{d}^k\mathfrak{u}\right) = 0.$$

Especially, if $\mathrm{d}^k\mathfrak{u}\,(t=0) = 0$, then for all time, $\mathrm{d}^k\mathfrak{u} = 0$.

Considering now the *Lie co-derivative* $\mathcal{L}_{\mathbf{b}}$, defined as

$$\begin{array}{rccc} \mathcal{L}_{\mathbf{b}} & : & C^\infty\Lambda^k & \longmapsto & C^\infty\Lambda^k \\ & & \mathfrak{u} & \longmapsto & \mathcal{L}_{\mathbf{b}}\,\mathfrak{u} = j_{\mathbf{b}} \circ \delta^k\mathfrak{u} + \delta^{k+1} \circ j_{\mathbf{b}}\mathfrak{u}. \end{array}$$

the adjoint Lie advection problem

$$\partial_t \mathfrak{u} - \mathcal{L}_{\mathbf{b}}\,\mathfrak{u} = 0, \tag{19}$$

can be considered. Then similar properties as for (18) can be proven for $\delta^k\mathfrak{u}$ instead of $\mathrm{d}^k\mathfrak{u}$.

Written with proxies on $C^\infty\Lambda^1$, equations (18) and (19) lead to two equations

- The first one is

$$\partial_t \mathbf{u} + \nabla\left(\mathbf{b} \cdot \mathbf{u}\right) + \mathbf{b}^\perp\nabla^\perp \cdot \mathbf{u} = 0,$$

  and is (18) with the choice of proxy (1), and is also (19) with the choice of proxy (2). $\nabla^\perp \cdot \mathbf{u}$ follows the conservative equation

$$\partial_t\left(\nabla^\perp \cdot \mathbf{u}\right) + \nabla \cdot \left(\left(\nabla^\perp \cdot \mathbf{u}\right)\mathbf{b}\right) = 0.$$

  If $\nabla^\perp \cdot \mathbf{u}\,(t=0) = 0$, then $\nabla^\perp \cdot \mathbf{u} = 0$ for any $t > 0$. It can be encountered in the equation on $\mathbf{w}$ in the two-phase flows model of [60], which was for example numerically addressed in [59].

- The second one is the two dimensional *induction equation*

$$\partial_t \mathbf{u} + \nabla^\perp\left(\det(\mathbf{b}, \mathbf{u})\right) + \mathbf{b}\nabla \cdot \mathbf{u} = 0, \tag{20}$$

  obtained with (19) with the choice of proxy (1), and is also (18) with the choice of proxy (2). Then $\nabla \cdot \mathbf{u}$ follows the conservative equation

$$\partial_t\left(\nabla \cdot \mathbf{u}\right) + \nabla \cdot \left(\left(\nabla \cdot \mathbf{u}\right)\mathbf{b}\right) = 0. \tag{21}$$

  If $\nabla \cdot \mathbf{u}\,(t=0) = 0$, then $\nabla \cdot \mathbf{u} = 0$ for any $t > 0$.

5.2 Discretization

We are interested in the discretization of (20). This equation can be seen either as the equation (18) with the proxy (2), or as the equation (19) with the proxy (1). In Proposition 5, we proved that $(\nabla)^\star$ could be preserved by the discontinuous Galerkin method provided the approximation space is $\mathbf{d}\mathbb{B}_k^{\mathrm{curl}}$ and the numerical flux is tangential to the normal. This suggests to see the equation (20) as the equation (19) with the proxy (1). This leads to the following numerical scheme:

$$\begin{aligned}&\text{find } \mathbf{u} \in \mathbf{d}\mathbb{B}_k^{\mathrm{curl}} \text{ such that for all } \mathbf{v} \in \mathbf{d}\mathbb{B}_k^{\mathrm{curl}}\\ &\sum_{c\in\mathcal{C}}\int_c \mathbf{v}\cdot\partial_t\mathbf{u} - \sum_{c\in\mathcal{C}}\int_c \det(\mathbf{b},\mathbf{u})\,\nabla^\perp\cdot\mathbf{v} + \sum_{S\in\mathcal{S}}\int_S [\![\mathbf{v}]\!]\cdot\widetilde{\mathbf{G}} + \sum_{c\in\mathcal{C}}\int_c \mathbf{v}\cdot\mathbf{b}\,(-\nabla^\star\mathbf{u}) = 0,\end{aligned} \tag{22}$$

for which we can prove

Proposition 6 (Equation on $-\nabla^\star\mathbf{u}$)**.** *If* $\mathbf{u}$ *is solution of* (22)*, and if the numerical flux is orthogonal to* $\mathbf{n}$*, then* $-\nabla^\star\mathbf{u}$ *is solution of the continuous Galerkin discretization for the advection equation on the divergence* (21)

$$\textit{Find } D\in\mathbb{A}_{k+1} \quad \forall f\in\mathbb{A}_{k+1} \qquad \sum_{c\in\mathcal{C}}\int_c f\partial_t D - \sum_{c\in\mathcal{C}}\int_c D\mathbf{b}\cdot\nabla f = 0. \tag{23}$$

Proof. We consider (22), which is tested with $\mathbf{v}=\nabla f$, where $f\in\mathbb{A}_{k+1}$. Then

$$\nabla^\perp\cdot\mathbf{v} = \nabla^\perp\cdot(\nabla f) = 0.$$

As $\widetilde{\mathbf{G}}$ is orthogonal to $\mathbf{n}$, it may be rewritten $\tilde{g}\mathbf{n}^\perp$. This leads to

$$[\![\mathbf{v}]\!]\cdot\widetilde{\mathbf{G}} = [\![\mathbf{v}]\!]\cdot\tilde{g}\mathbf{n}^\perp = [\![\mathbf{v}\cdot\mathbf{n}^\perp]\!]\,\tilde{g},$$

and if $f\in\mathbb{A}_{k+1}$, then $[\![\nabla f\cdot\mathbf{n}^\perp]\!]=0$. Therefore (22) tested with ∇f for $f\in\mathbb{A}_{k+1}$ gives

$$\forall f\in\mathbb{A}_{k+1} \qquad \sum_{c\in\mathcal{C}}\int_c \nabla f\cdot\partial_t\mathbf{u} + \sum_{c\in\mathcal{C}}\int_c \nabla f\cdot\mathbf{b}\,(-\nabla^\star\mathbf{u}) = 0. \tag{24}$$

The time derivative term may be transformed as (the commutation between $\nabla^\star$ and ∂_t can be proven as in the proof of Proposition 4):

$$\begin{aligned}\sum_{c\in\mathcal{C}}\int_c \nabla f\cdot\partial_t\mathbf{u} &= \langle\nabla f|\partial_t\mathbf{u}\rangle_{\mathbf{d}\mathbb{B}_k^{\mathrm{curl}}}\\ &= \langle f|\nabla^\star(\partial_t\mathbf{u})\rangle_{\mathbb{A}_{k+1}}\\ &= \langle f|\partial_t\nabla^\star(\mathbf{u})\rangle_{\mathbb{A}_{k+1}}\\ \sum_{c\in\mathcal{C}}\int_c \nabla f\cdot\partial_t\mathbf{u} &= -\langle f|\partial_t(-\nabla^\star(\mathbf{u}))\rangle_{\mathbb{A}_{k+1}}.\end{aligned}$$

Equation (24) becomes finally

$$\forall f\in\mathbb{A}_{k+1} \qquad \sum_{c\in\mathcal{C}}\int_c f\partial_t(-\nabla^\star(\mathbf{u})) - \sum_{c\in\mathcal{C}}\int_c \nabla f\cdot\mathbf{b}\,(-\nabla^\star\mathbf{u}) = 0,$$

which means that $(-\nabla^\star\mathbf{u})$ is solution of (23). □

Note that $-\nabla^\star\mathbf{u}$ is solution of the numerical scheme (23), which is known to be unstable. However, it will be used in practical applications with initial condition $\nabla^\star\mathbf{u}(t=0)=0$, so that this instability should not raise any problem provided the initialization is carefully performed.

Proposition 7 (Exact preservation of $\nabla^\star\mathbf{u}=0$)**.** *We consider equation* (20)*. Suppose that* $\mathbf{u}(t=0)=\mathbf{u}^0$ *derives from a potential* f^0*:* $\mathbf{u}^0=\nabla^\perp f^0$*, and we denote by* f_h^0 *the projection of* f^0 *in* $\mathbb{C}_k$*. Then* $\mathbf{u}_h^0 := -\left(\nabla^\perp_{\mathscr{D}},\cdot\right)^\star f_h^0$ *is such that* $\nabla^\star\mathbf{u}_h^0=0$*, and under hypothesis of Proposition 6, the constraint* $\nabla^\star\mathbf{u}_h=0$ *is preserved for all time by the numerical scheme* (22)*.*

Proof. The beginning of the proof relies only on relations between the kernel and range of an operator and its adjoint. Note that we are working here in finite dimension, so that these relations do not include closures of range or kernel.

If $f \in \mathbb{C}_k$, then $\left(\nabla^\perp_{\mathscr{D}'}\cdot\right)^\star f \in \left(\ker\left(\nabla^\perp_{\mathscr{D}'}\cdot\right)\right)^\perp$. But as $\operatorname{Range}\nabla \subset \ker\left(\nabla^\perp_{\mathscr{D}'}\cdot\right)$, we also have $\left(\nabla^\perp_{\mathscr{D}'}\cdot\right)^\star f \in (\operatorname{Range}\nabla)^\perp$. As $(\operatorname{Range}\nabla)^\perp = \ker\nabla^\star$, we have $\left(\nabla^\perp_{\mathscr{D}'}\cdot\right)^\star f \in \ker\nabla^\star$, and so $\nabla^\star\mathbf{u}_h^0 = 0$.

Then by Proposition 6, $\nabla^\star\mathbf{u}_h$ ensures the numerical scheme (23) which preserves $\nabla^\star\mathbf{u}_h = 0$ for all time, which ends the proof. □

Remark 6 (Divergence free initialization)**.** We provide some details about how the initial condition is computed. Usually, the computation of the initial condition $\mathbf{u}_0^h$ is computed by projection of the initial condition $\mathbf{u}_0$ on the finite element space. This leads to the following system to solve

$$M\mathbf{u}_0^h = \mathbf{RHS},$$

where M is the mass matrix of the finite element space of the velocity space: if $\mathbf{v}$ denotes a basis of this finite element basis, the mass matrix is

$$M_{i,j} = \int_\Omega \mathbf{v}_i \cdot \mathbf{v}_j, \tag{25}$$

and **RHS** is the right hand side, equal to

$$\mathbf{RHS}_i = \int_\Omega \mathbf{u}_0 \cdot \mathbf{v}_i. \tag{26}$$

Suppose now that the initial condition derives from a potential vector f: $\mathbf{u}_0 = \nabla^\perp_{\mathscr{D}'} f$. Then at the discrete level, we wish to have $\mathbf{u}_0^h = -\left(\nabla^\perp_{\mathscr{D}'}\cdot\right)^\star f$, namely

$$\forall \mathbf{v} \in \mathbf{d}\mathbb{B}_k^{\mathrm{curl}} \qquad \left\langle \mathbf{u}_0^h | \mathbf{v} \right\rangle_{\mathbf{d}\mathbb{B}_k^{\mathrm{div}}} = -\left\langle \left(\nabla^\perp_{\mathscr{D}'}\cdot\right)^\star f | \mathbf{v} \right\rangle_{\mathbf{d}\mathbb{B}_k^{\mathrm{div}}} = -\left\langle f | \nabla^\perp_{\mathscr{D}'} \cdot \mathbf{v} \right\rangle_{\mathbf{d}\mathbb{B}_k^{\mathrm{div}}}.$$

This gives

$$\forall \mathbf{v} \in \mathbf{d}\mathbb{B}_k^{\mathrm{curl}} \qquad \left\langle \mathbf{u}_0^h | \mathbf{v} \right\rangle_{\mathbf{d}\mathbb{B}_k^{\mathrm{div}}} = -\sum_{c\in\mathcal{C}} \int_c f \nabla^\perp_{\mathscr{D}'} \cdot \mathbf{v} + \sum_{S\in\mathcal{S}} \int_S f \left[\!\left[\mathbf{v} \cdot \mathbf{n}^\perp \right]\!\right].$$

Therefore, the matrix of the system to solve is still (25), but the right hand side is no more (26), but

$$\mathbf{RHS}_i = -\sum_{c\in\mathcal{C}} \int_c f \nabla^\perp_{\mathscr{D}'} \cdot \mathbf{v}_i + \sum_{S\in\mathcal{S}} \int_S f \left[\!\left[\mathbf{v}_i \cdot \mathbf{n}^\perp \right]\!\right].$$

6 Numerical results

For all the numerical tests, the computational domain is the periodic square domain $[0,1]^2$. We will consider three types of mesh: Cartesian, unstructured quadrangular and unstructured triangular. The meshes on which the conservation tests will be performed are represented in Figure 3.

The convergence tests will be performed on Cartesian meshes with uniform size of the mesh, with $h = 0.1$, $h = 0.05$, $h = 0.025$ and $h = 0.0125$. The convergence tests on triangular meshes will be performed on a set of unstructured meshes with a number of cells equal to 268, 1036, 4186 and 16682, and minimal size (defined as the square root of the surface of the smallest element) approximately equal to 0.0844, 0.0419, 0.0223 and 0.0109.

For all the test cases, the time stepping is done with classical Strong-Stability Preserving explicit time schemes [31]. If k is the polynomial order of the space discretization, the order of the time integration scheme is $k+1$. The CFL number is equal to 0.5 for $k = 0$, 0.33 for $k = 1$ and 0.2 for $k = 2$.

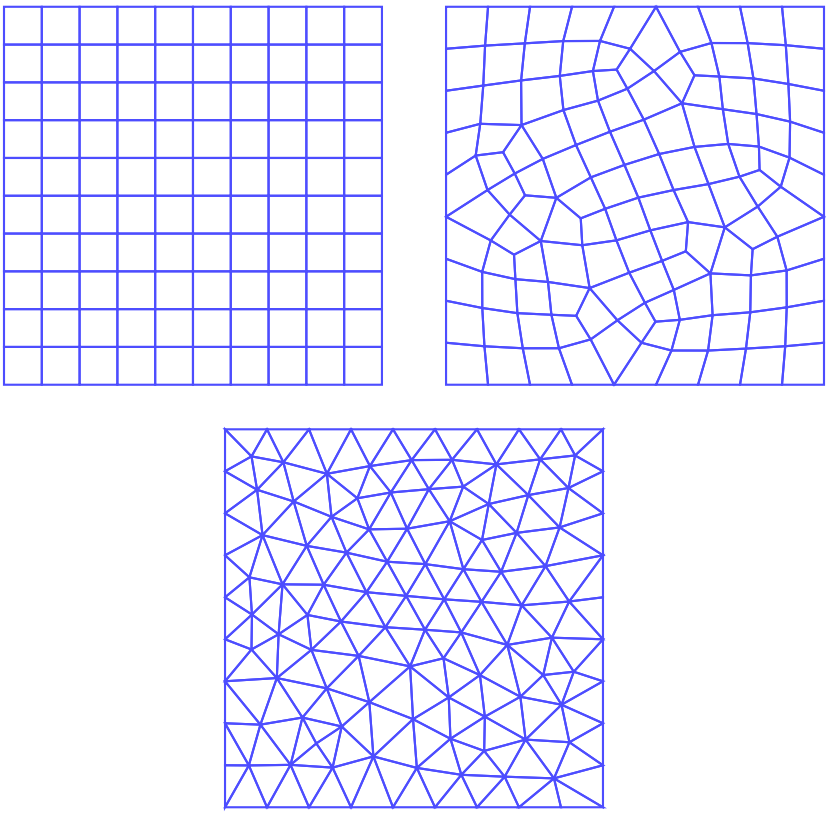

Figure 3: The meshes on which the conservation of divergence or curl are performed. Top left: Cartesian mesh, top right: unstructured quadrangular mesh, bottom: unstructured triangular mesh.

6.1 Discrete conservation of the divergence: Maxwell system

In this section, we are interested in the two-dimensional Maxwell system in the vacuum, which reads

$$\begin{cases} \partial_t b + \nabla^\perp \cdot \mathbf{e} = 0 \\ \partial_t \mathbf{e} + c^2 \nabla^\perp b = 0, \end{cases} \tag{27}$$

where $\mathbf{e}$ is the two-dimensional electric field and b is the z-component of the magnetic field.

6.1.1 Conservation of the divergence of a stationary solution

For this first test case, the following initial condition is imposed

$$\begin{cases} b(\mathbf{x}) = 0 \\ \mathbf{e}_x(\mathbf{x}) = \overline{x}\, \mathrm{e}^{-\overline{r}^2/2} \\ \mathbf{e}_y(\mathbf{x}) = \overline{y}\, \mathrm{e}^{-\overline{r}^2/2}, \end{cases}$$

with $\overline{x} = \dfrac{x - x_c}{r_0}$, $\overline{y} = \dfrac{y - y_c}{r_0}$, $r^2 = (x - x_c)^2 + (y - y_c)^2$, and $\overline{r} = \dfrac{r}{r_0}$. This initial condition is such that $\nabla^\perp \cdot \mathbf{e} = 0$, and so is clearly a stationary solution of (27). This solution was built by considering the potential $\mathrm{e}^{-\overline{r}^2/2}$ and by taking its gradient. The numerical parameters are $r_0 = 0.15$, $x_c = y_c = 0.5$, and $c^2 = 1$. The computation is led until $t = 3$ on the different meshes represented in Figure 3, and The L^2 difference between $\nabla^\star \mathbf{e}$ and its initial value is computed along the time. Two configurations of finite element spaces for approximating $\mathbf{e}$ are used:

- the finite element spaces $\mathbf{d}\mathbb{B}_k^{\mathrm{curl}}$,
- the classical finite element spaces for discontinuous Galerkin methods obtained by tensorization of the scalar basis (note however that in the triangular case, these two approximation spaces match),

and with two different numerical flux:

- the Lax-Friedrich flux,
- the Lax-Friedrich flux with purely tangential diffusion (17), which matches in our case with the Godunov' flux.

Numerical results are represented in Figure 4 for degree $k = 0, 1, 2$, and show that the only combination that preserves correctly the divergence is the one with the finite element space $\mathbf{d}\mathbb{B}_k^{\mathrm{curl}}$ and with the Godunov' numerical flux.

6.1.2 Convergence test

The numerical test is taken from [49, Section 5.1]. The initial condition is

$$\begin{cases} b(\mathbf{x}) = \dfrac{\omega}{c^2} \cos(k_\perp \pi y) \sin(k_\parallel \pi x) \\ \mathbf{e}_x(\mathbf{x}) = -k_\perp \pi \sin(k_\perp \pi y) \cos(k_\parallel \pi x) \\ \mathbf{e}_y(\mathbf{x}) = k_\parallel \pi \cos(k_\perp \pi y) \sin(k_\parallel \pi x) \end{cases} \tag{28}$$

and the exact solution is

$$\begin{cases} b(\mathbf{x}, t) = \dfrac{\omega}{c^2} \cos(k_\perp \pi y) \sin(k_\parallel \pi x - \omega t) \\ \mathbf{e}_x(\mathbf{x}, t) = -k_\perp \pi \sin(k_\perp \pi y) \cos(k_\parallel \pi x - \omega t) \\ \mathbf{e}_y(\mathbf{x}, t) = k_\parallel \pi \cos(k_\perp \pi y) \sin(k_\parallel \pi x - \omega t) \end{cases}$$

The longitudinal and transverse wave numbers $k_\parallel$ and $k_\perp$ are data of the test case. The frequency ω is such that

$$k_\parallel^2 + k_\perp^2 = \frac{\omega^2}{\pi^2 c^2}.$$

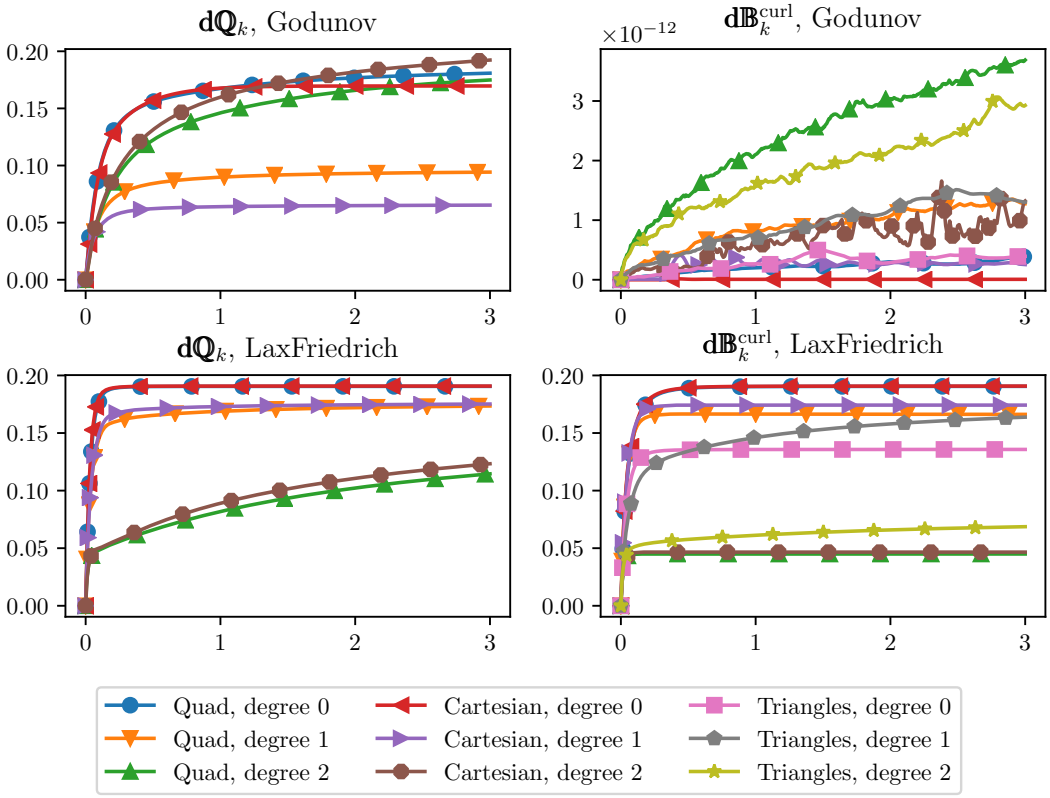

Figure 4: Plot of $\|\nabla^\star \mathbf{e} - \nabla^\star \mathbf{e}_0\|_2$ with respect to time for different degree, approximation space, type of meshes and numerical flux. In the left column, Cartesian and unstructured quadrangular meshes are considered, with the $\mathbf{d}\mathbb{Q}_k$ approximation space with the Godunov (top figure) and Lax-Friedrich (bottom figure) numerical flux. In the right column, Cartesian, unstructured quadrangular and triangular meshes are considered, with the $\mathbf{d}\mathbb{B}_k^{\mathrm{curl}}$ approximation space with the Godunov (top figure) and Lax-Friedrich (bottom figure) numerical flux. On triangular meshes, the space $\mathbf{d}\mathbb{B}_k^{\mathrm{curl}}$ and $\mathbf{d}\mathbb{P}_k$ are the same, and the computations on these spaces are represented on the right column. Note that the y scaling of the top right figure ($\mathbf{d}\mathbb{B}_k^{\mathrm{curl}}$ with Godunov' scheme) is 10^{-12}, whereas it is of the order of 1 for the other plots.

	Godunov				Lax-Friedrich			
	$\mathbf{d}\mathbb{Q}_0$		$\mathbf{d}\mathbb{B}_0^{\text{curl}}$		$\mathbf{d}\mathbb{Q}_0$		$\mathbf{d}\mathbb{B}_0^{\text{curl}}$	
h	Error	rate	Error	rate	Error	rate	Error	rate
0.1	2.76e+00		2.76e+00		2.99e+00		2.99e+00	
0.05	2.02e+00	0.45	2.02e+00	0.45	2.44e+00	0.30	2.44e+00	0.30
0.025	1.26e+00	0.68	1.26e+00	0.68	1.65e+00	0.56	1.65e+00	0.56
0.0125	7.08e-01	0.83	7.08e-01	0.83	9.76e-01	0.76	9.76e-01	0.76

	Godunov				Lax-Friedrich			
	$\mathbf{d}\mathbb{Q}_1$		$\mathbf{d}\mathbb{B}_1^{\text{curl}}$		$\mathbf{d}\mathbb{Q}_1$		$\mathbf{d}\mathbb{B}_1^{\text{curl}}$	
h	Error	rate	Error	rate	Error	rate	Error	rate
0.1	1.84e-01		1.54e-01		1.75e-01		1.54e-01	
0.05	4.23e-02	2.12	3.57e-02	2.11	3.88e-02	2.17	3.57e-02	2.11
0.025	1.04e-02	2.03	8.72e-03	2.03	9.28e-03	2.06	8.72e-03	2.03
0.0125	2.60e-03	2.00	2.17e-03	2.01	2.29e-03	2.02	2.17e-03	2.01

	Godunov				Lax-Friedrich			
	$\mathbf{d}\mathbb{Q}_2$		$\mathbf{d}\mathbb{B}_2^{\text{curl}}$		$\mathbf{d}\mathbb{Q}_2$		$\mathbf{d}\mathbb{B}_2^{\text{curl}}$	
h	Error	rate	Error	rate	Error	rate	Error	rate
0.1	6.41e-03		4.90e-03		7.17e-03		5.98e-03	
0.05	8.16e-04	2.97	6.08e-04	3.01	9.32e-04	2.94	7.61e-04	2.97
0.025	1.03e-04	2.98	7.59e-05	3.00	1.19e-04	2.97	9.57e-05	2.99
0.0125	1.30e-05	2.99	9.48e-06	3.00	1.49e-05	2.99	1.20e-05	3.00

Table 2: Errors and convergence rates obtained on the variable $\mathbf{e}_x$ with the test case described in subsubsection 6.1.2 with initial condition (28), on a series of triangular meshes. Results show a low benefit in using the Godunov flux, namely in exactly preserving the divergence.

The numerical parameters are $c = 1$, and $k_{\|} = k_{\perp} = 2$.

A second test case is performed, in which a stationary non divergence free solution is added to the initial solution (28) (it is similar to the stationary solution of subsubsection 6.1.1, but regular), equal to

$$\begin{cases} b(\mathbf{x}) = 0 \\ \mathbf{e}_x(\mathbf{x}) = 2K_0\,\alpha\,\overline{x}\,\dfrac{\mathrm{e}^{-\alpha/(1-\overline{r}^2)}}{(1-\overline{r}^2)^2} \\ \mathbf{e}_y(\mathbf{x}) = 2K_0\,\alpha\,\overline{y}\,\dfrac{\mathrm{e}^{-\alpha/(1-\overline{r}^2)}}{(1-\overline{r}^2)^2}, \end{cases} \tag{29}$$

if $r < r_0$, and 0 otherwise. The numerical parameters are $K_0 = 100$, $r_0 = 0.35$, $x_c = y_c = 0.5$, $\alpha = 4$.

The convergence curves obtained on the two test cases on each variable is plotted in Figure 5. The errors obtained and rate of convergence for Cartesian meshes on the variable $\mathbf{e}_x$ are gathered in Table 2 for the case with the initial condition (28) and in Table 2 where (29) was added to the initial condition (28). With the single initial condition (28), the order of convergence obtained is very few sensitive to the change of approximation basis or of the change of numerical flux. This is probably due to the fact that (28) is already divergence free, and so the numerical divergence is already low when computing the initial condition, and so the benefit of preserving exactly the divergence by using the space $\mathbf{d}\mathbb{B}_k^{\text{curl}}$ with Godunov flux is low.

The same plots are performed on the series of triangular meshes, shown in Figure 6, and the errors obtained for the variable $\mathbf{e}_x$ are shown in Table 4 and Table 5. The same observation as for Cartesian meshes hold.

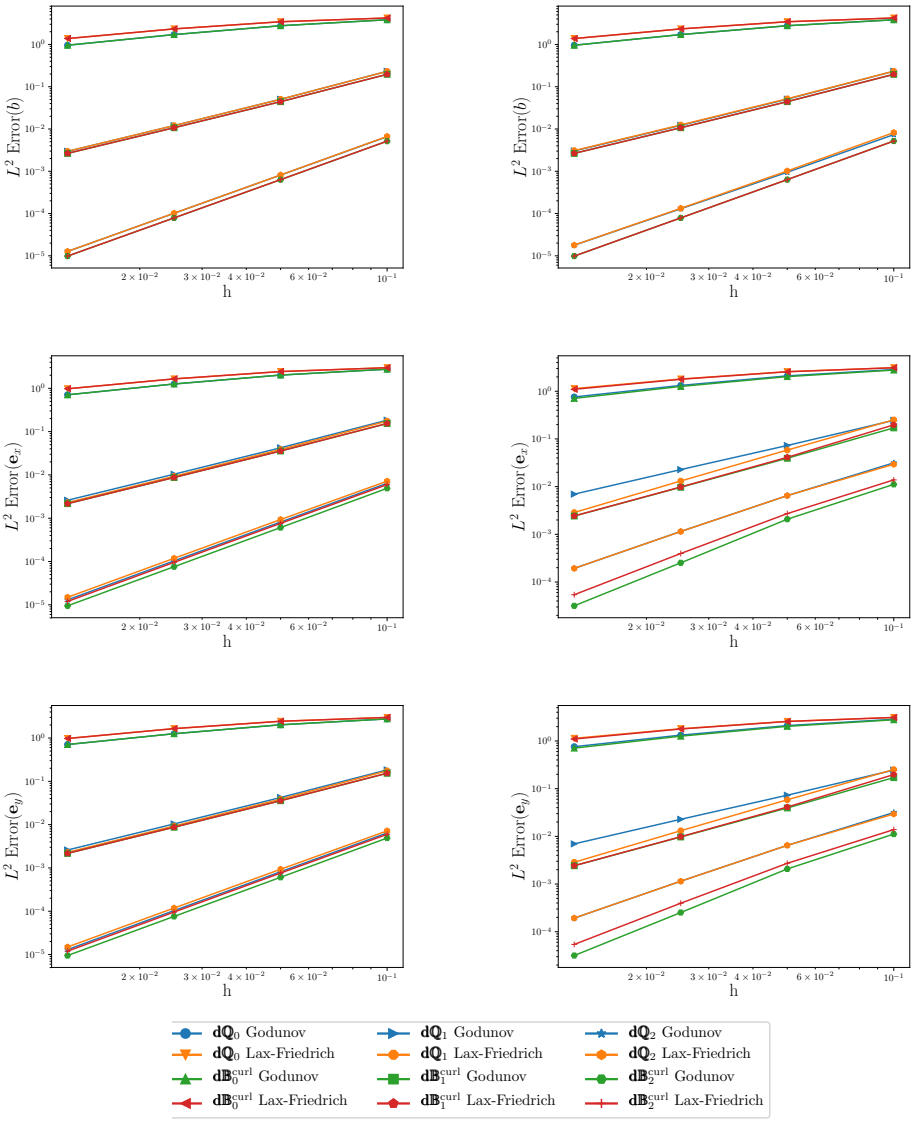

Figure 5: Error obtained on the test case described in subsubsection 6.1.2 with initial condition (28) on the left, and with the initial condition (29) added to (28) on the right, on a series of Cartesian meshes. For each of the test cases, the error obtained for the variables b (top row), $\mathbf{e}_x$ (middle row) and $\mathbf{e}_y$ (bottom row) is shown for different approximation spaces and for the Lax-Friedrich and Godunov flux.

	Godunov				Lax-Friedrich			
	$\mathbf{d}\mathbb{Q}_0$		$\mathbf{d}\mathbb{B}_0^{\mathrm{curl}}$		$\mathbf{d}\mathbb{Q}_0$		$\mathbf{d}\mathbb{B}_0^{\mathrm{curl}}$	
h	Error	rate	Error	rate	Error	rate	Error	rate
0.1	2.85e+00		2.78e+00		3.12e+00		3.11e+00	
0.05	2.10e+00	0.44	2.03e+00	0.46	2.58e+00	0.27	2.56e+00	0.28
0.025	1.33e+00	0.66	1.26e+00	0.69	1.81e+00	0.51	1.78e+00	0.52
0.0125	7.59e-01	0.81	7.09e-01	0.83	1.14e+00	0.67	1.10e+00	0.70
	Godunov				Lax-Friedrich			
	$\mathbf{d}\mathbb{Q}_1$		$\mathbf{d}\mathbb{B}_1^{\mathrm{curl}}$		$\mathbf{d}\mathbb{Q}_1$		$\mathbf{d}\mathbb{B}_1^{\mathrm{curl}}$	
h	Error	rate	Error	rate	Error	rate	Error	rate
0.1	2.45e-01		1.71e-01		2.52e-01		1.98e-01	
0.05	7.29e-02	1.75	3.94e-02	2.12	5.84e-02	2.11	4.11e-02	2.26
0.025	2.28e-02	1.68	9.70e-03	2.02	1.31e-02	2.15	9.83e-03	2.07
0.0125	6.96e-03	1.71	2.42e-03	2.00	2.87e-03	2.20	2.43e-03	2.02
	Godunov				Lax-Friedrich			
	$\mathbf{d}\mathbb{Q}_2$		$\mathbf{d}\mathbb{B}_2^{\mathrm{curl}}$		$\mathbf{d}\mathbb{Q}_2$		$\mathbf{d}\mathbb{B}_2^{\mathrm{curl}}$	
h	Error	rate	Error	rate	Error	rate	Error	rate
0.1	3.15e-02		1.12e-02		2.94e-02		1.38e-02	
0.05	6.47e-03	2.29	2.07e-03	2.43	6.48e-03	2.18	2.72e-03	2.35
0.025	1.15e-03	2.50	2.53e-04	3.04	1.14e-03	2.50	3.96e-04	2.78
0.0125	1.93e-04	2.57	3.17e-05	3.00	1.93e-04	2.57	5.41e-05	2.87

Table 3: Errors and convergence rates obtained on the variable $\mathbf{e}_x$ with the test case described in subsubsection 6.1.2 with initial condition (28), on a series of Cartesian meshes. Results show a high benefit in using the space $\mathbf{d}\mathbb{B}_k^{\mathrm{curl}}$ with the Godunov flux, which is the only one to always reach the optimal order.

	Godunov		Lax-Friedrich	
h	Error	rate	Error	rate
0.08439823	2.39e+00		2.70e+00	
0.04187874	1.58e+00	0.59	1.93e+00	0.47
0.02226197	9.25e-01	0.85	1.19e+00	0.77
0.01091023	4.94e-01	0.88	6.58e-01	0.83
	Godunov		Lax-Friedrich	
h	Error	rate	Error	rate
0.08439823	1.43e-01		1.54e-01	
0.04187874	2.92e-02	2.27	3.15e-02	2.27
0.02226197	6.47e-03	2.38	7.43e-03	2.29
0.01091023	1.53e-03	2.02	1.98e-03	1.85
	Godunov		Lax-Friedrich	
h	Error	rate	Error	rate
0.08439823	7.53e-03		8.83e-03	
0.04187874	9.22e-04	3.00	1.28e-03	2.75
0.02226197	1.10e-04	3.37	1.76e-04	3.14
0.01091023	1.30e-05	2.99	2.49e-05	2.75

Table 4: Errors and convergence rates obtained on the variable $\mathbf{e}_x$ with the test case described in subsubsection 6.1.2 with initial condition (28), on the series of triangular meshes. Results show a low benefit in using the Godunov flux, namely in exactly preserving the divergence.

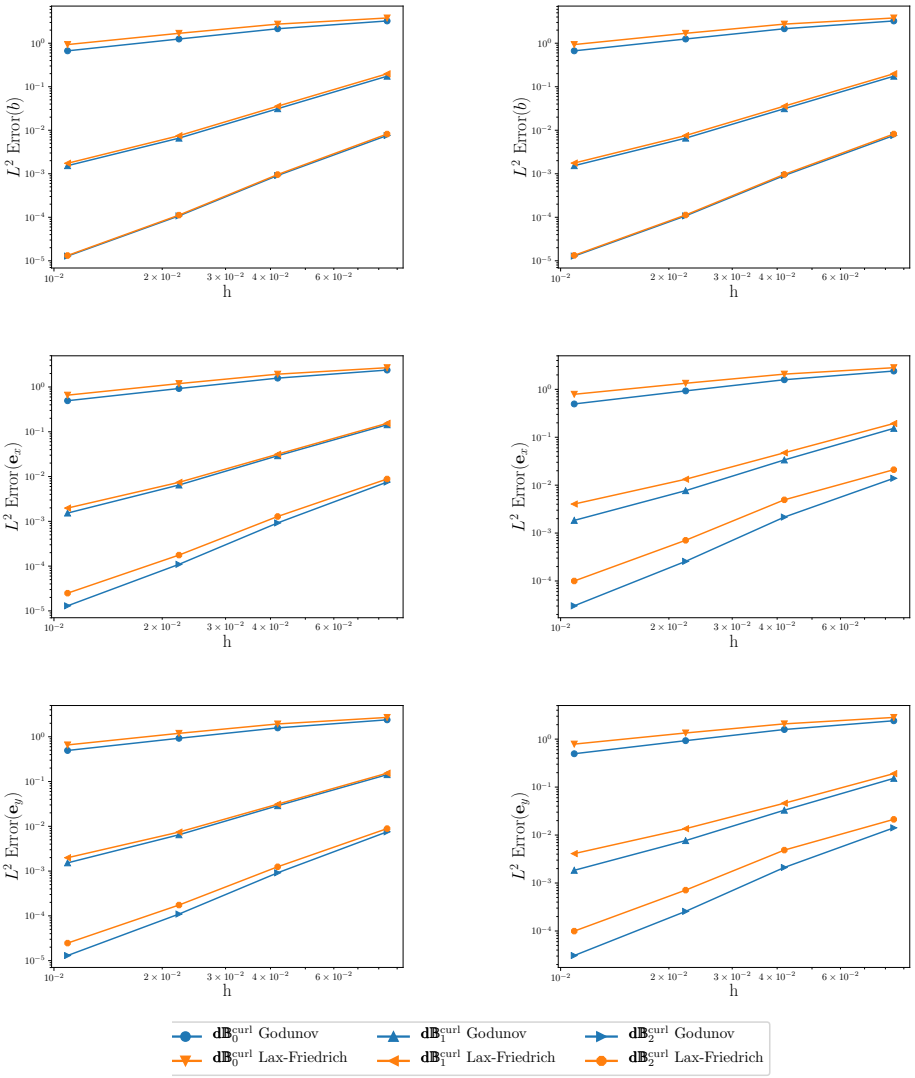

Figure 6: Error obtained on the test case described in subsubsection 6.1.2 with initial condition (28) on the left, and with the initial condition (29) added to (28) on the right, on a series of unstructured triangular meshes. For each of the test cases, the error obtained for the variables b (top row), $\mathbf{e}_x$ (middle row) and $\mathbf{e}_y$ (bottom row) is shown for different degrees, and for the Lax-Friedrich and Godunov numerical flux.

	Godunov		Lax-Friedrich	
h	Error	rate	Error	rate
0.08439823	2.41e+00		2.83e+00	
0.04187874	1.59e+00	0.60	2.08e+00	0.44
0.02226197	9.28e-01	0.85	1.34e+00	0.70
0.01091023	4.95e-01	0.88	7.88e-01	0.74
	Godunov		Lax-Friedrich	
h	Error	rate	Error	rate
0.08439823	1.53e-01		1.94e-01	
0.04187874	3.36e-02	2.17	4.74e-02	2.01
0.02226197	7.67e-03	2.34	1.33e-02	2.01
0.01091023	1.84e-03	2.00	4.04e-03	1.67
	Godunov		Lax-Friedrich	
h	Error	rate	Error	rate
0.08439823	1.39e-02		2.10e-02	
0.04187874	2.15e-03	2.66	4.94e-03	2.07
0.02226197	2.57e-04	3.37	7.07e-04	3.08
0.01091023	3.03e-05	3.00	9.99e-05	2.74

Table 5: Errors and convergence rates obtained on the variable $\mathbf{e}_x$ with the test case described in subsubsection 6.1.2 with initial condition (28), on the series of triangular meshes. Results show a higher benefit than in Table 4 in using the Godunov flux for preserving exactly the divergence.

6.2 Discrete conservation of a curl: Wave system

In this section, the wave system

$$\begin{cases} \partial_t p + \nabla \cdot \mathbf{u} = 0 \\ \partial_t \mathbf{u} + c^2 \nabla p = 0, \end{cases} \tag{30}$$

which couples the pressure p and the velocity $\mathbf{u}$ is considered. The wave velocity c is a parameter of the system, and will be always equal to 1 in the numerical applications.

6.2.1 Conservation of the curl of a stationary solution

For this first test case, the following initial condition is imposed

$$\begin{cases} p(\mathbf{x}) = 0 \\ \mathbf{u}_x(\mathbf{x}) = -\overline{y}\, \mathrm{e}^{-\overline{r}^2/2} \\ \mathbf{u}_y(\mathbf{x}) = \overline{x}\, \mathrm{e}^{-\overline{r}^2/2}, \end{cases}$$

with $\overline{x} = \dfrac{x - x_c}{r_0}$, $\overline{y} = \dfrac{y - y_c}{r_0}$, $r^2 = (x - x_c)^2 + (y - y_c)^2$, and $\overline{r} = \dfrac{r}{r_0}$. This initial condition is such that $\nabla \cdot \mathbf{u} = 0$, and so is clearly a stationary solution of (30). This solution was built by considering the potential $\mathrm{e}^{-\overline{r}^2/2}$ and by taking its rotated gradient $\nabla^\perp$. The numerical parameters are $r_0 = 0.15$, and $x_c = y_c = 0.5$. The computation is led until $t = 3$ on the different meshes represented in Figure 3, and The L^2 difference between $\left(\nabla^\perp\right)^\star \mathbf{u}$ and its initial value is computed along the time. Two configurations of finite element spaces for approximating $\mathbf{u}$ are used:

- the finite element spaces $\mathbf{dBB}_k^{\mathrm{div}}$,
- the classical finite element spaces for discontinuous Galerkin methods obtained by tensorization of the scalar basis (note however that in the triangular case, these two approximation spaces match),

and with two different numerical flux:

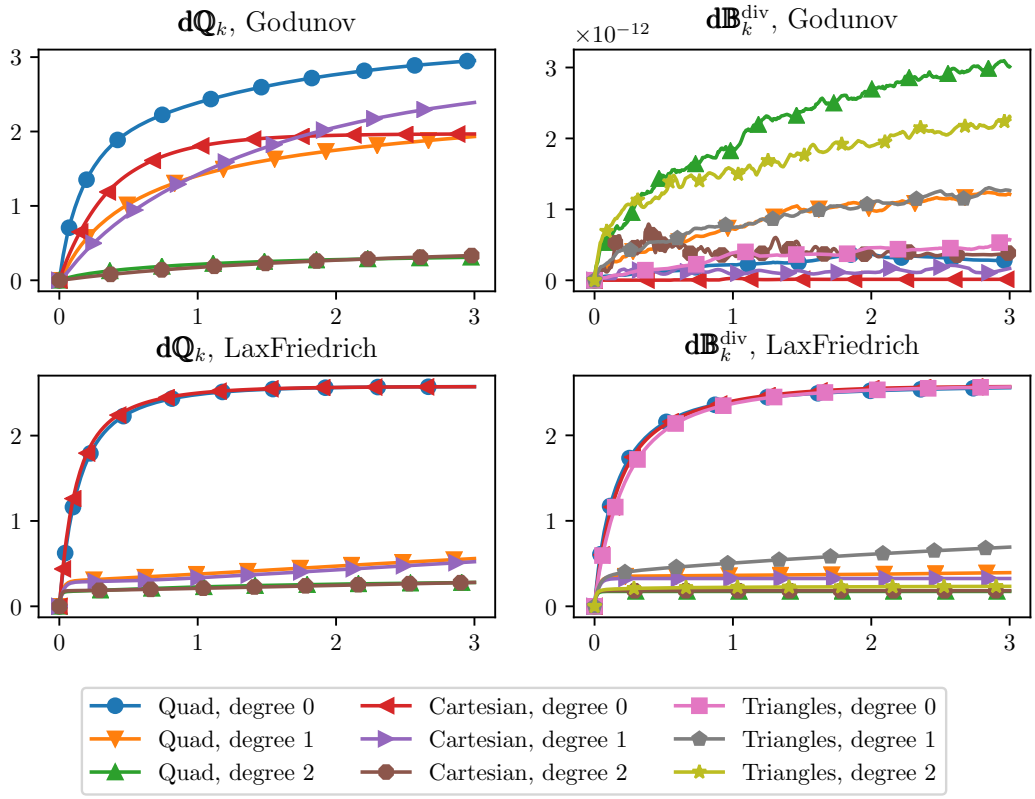

Figure 7: Plot of $\| \left(\nabla^{\perp}\right)^{\star} \mathbf{u} - \left(\nabla^{\perp}\right)^{\star} \mathbf{u}_0 \|_2$ with respect to time for different degree, approximation space, type of meshes and numerical flux. In the left column, Cartesian and unstructured quadrangular meshes are considered, with the $\mathbf{d}\mathbb{Q}_k$ approximation space with the Godunov (top figure) and Lax-Friedrich (bottom figure) numerical flux. In the right column, Cartesian, unstructured quadrangular and triangular meshes are considered, with the $\mathbf{d}\mathbb{B}_k^{\mathrm{div}}$ approximation space with the Godunov (top figure) and Lax-Friedrich (bottom figure) numerical flux. On triangular meshes, the space $\mathbf{d}\mathbb{B}_k^{\mathrm{div}}$ and $\mathbf{d}\mathbb{P}_k$ are the same, and the computations on these spaces are represented only on the right column. Note that the y scaling of the top right figure ($\mathbf{d}\mathbb{B}_k^{\mathrm{div}}$ with Godunov' scheme) is 10^{-12}, whereas it is of the order of 1 for the other plots.

- the Lax-Friedrich flux,
- the Lax-Friedrich flux with purely normal diffusion (14), which matches in our case with the Godunov' flux.

Numerical results are represented in Figure 7 for degree $k = 0, 1, 2$, and show that the only combination that preserves correctly the curl is the one with the finite element space $\mathbf{d}\mathbb{B}_k^{\mathrm{div}}$ and with the Godunov' numerical flux.

6.2.2 Convergence test

The numerical test is adapted from the one for the divergence convergence test case of subsubsection 6.1.2. The initial condition is

$$\begin{cases} p(\mathbf{x}) = \dfrac{\omega}{c^2} \sin\left(k_{\perp}\pi y\right) \cos\left(k_{\parallel}\pi x\right) \\ \mathbf{u}_x(\mathbf{x}) = k_{\parallel}\pi \cos\left(k_{\perp}\pi y\right) \sin\left(k_{\parallel}\pi x\right) \\ \mathbf{u}_y(\mathbf{x}) = k_{\perp}\pi \sin\left(k_{\perp}\pi y\right) \cos\left(k_{\parallel}\pi x\right) \end{cases} \tag{31}$$

	Godunov				Lax-Friedrich			
	$\mathbf{d}\mathbb{Q}_0$		$\mathbf{d}\mathbb{B}_0^{\text{div}}$		$\mathbf{d}\mathbb{Q}_0$		$\mathbf{d}\mathbb{B}_0^{\text{div}}$	
h	Error	rate	Error	rate	Error	rate	Error	rate
0.1	2.76e+00		2.76e+00		2.99e+00		2.99e+00	
0.05	2.02e+00	0.45	2.02e+00	0.45	2.44e+00	0.30	2.44e+00	0.30
0.025	1.26e+00	0.68	1.26e+00	0.68	1.65e+00	0.56	1.65e+00	0.56
0.0125	7.08e-01	0.83	7.08e-01	0.83	9.76e-01	0.76	9.76e-01	0.76

	Godunov				Lax-Friedrich			
	$\mathbf{d}\mathbb{Q}_1$		$\mathbf{d}\mathbb{B}_1^{\text{div}}$		$\mathbf{d}\mathbb{Q}_1$		$\mathbf{d}\mathbb{B}_1^{\text{div}}$	
h	Error	rate	Error	rate	Error	rate	Error	rate
0.1	1.84e-01		1.54e-01		1.75e-01		1.54e-01	
0.05	4.23e-02	2.12	3.57e-02	2.11	3.88e-02	2.17	3.57e-02	2.11
0.025	1.04e-02	2.03	8.72e-03	2.03	9.28e-03	2.06	8.72e-03	2.03
0.0125	2.60e-03	2.00	2.17e-03	2.01	2.29e-03	2.02	2.17e-03	2.01

	Godunov				Lax-Friedrich			
	$\mathbf{d}\mathbb{Q}_2$		$\mathbf{d}\mathbb{B}_2^{\text{div}}$		$\mathbf{d}\mathbb{Q}_2$		$\mathbf{d}\mathbb{B}_2^{\text{div}}$	
h	Error	rate	Error	rate	Error	rate	Error	rate
0.1	6.41e-03		4.90e-03		7.17e-03		5.98e-03	
0.05	8.16e-04	2.97	6.08e-04	3.01	9.32e-04	2.94	7.61e-04	2.97
0.025	1.03e-04	2.98	7.59e-05	3.00	1.19e-04	2.97	9.57e-05	2.99
0.0125	1.30e-05	2.99	9.48e-06	3.00	1.49e-05	2.99	1.20e-05	3.00

Table 6: Errors and convergence rates obtained on the variable $\mathbf{u}_x$ with the test case described in subsubsection 6.2.2 with initial condition (31), on a series of triangular meshes. Results show a low benefit in using the Godunov flux, namely in exactly preserving the divergence.

and the exact solution is

$$\begin{cases} p(\mathbf{x}) = \dfrac{\omega}{c^2} \sin\left(k_\perp \pi y - \omega t\right) \cos\left(k_\parallel \pi x\right) \\ \mathbf{u}_x(\mathbf{x}) = k_\parallel \pi \cos\left(k_\perp \pi y - \omega t\right) \sin\left(k_\parallel \pi x\right) \\ \mathbf{u}_y(\mathbf{x}) = k_\perp \pi \sin\left(k_\perp \pi y - \omega t\right) \cos\left(k_\parallel \pi x\right). \end{cases}$$

The longitudinal and transverse wave numbers $k_\parallel$ and $k_\perp$ are data of the test case. The frequency ω is such that

$$k_\parallel^2 + k_\perp^2 = \frac{\omega^2}{\pi^2 c^2}.$$

The numerical parameters are $c = 1$, and $k_\parallel = k_\perp = 2$.

A second test case is performed, in which a stationary non curl free solution is added to the initial solution (31) (it is similar to the stationary solution of subsubsection 6.2.1, but regular), equal to

$$\begin{cases} b(\mathbf{x}) = 0 \\ \mathbf{u}_x(\mathbf{x}) = -2K_0\, \alpha\, \overline{y}\, \dfrac{\mathrm{e}^{-\alpha/(1-\overline{r}^2)}}{(1-\overline{r}^2)^2} \\ \mathbf{u}_y(\mathbf{x}) = 2K_0\, \alpha\, \overline{x}\, \dfrac{\mathrm{e}^{-\alpha/(1-\overline{r}^2)}}{(1-\overline{r}^2)^2}, \end{cases} \tag{32}$$

if $r < r_0$, and 0 otherwise. The numerical parameters are $K_0 = 100$, $r_0 = 0.35$, $x_c = y_c = 0.5$, $\alpha = 4$. The convergence curve for this test case with the two initial conditions are represented in Figure 8 for Cartesian meshes, and the matching table with the convergence errors and rates are summarized in Table 6 and Table 7. For triangular meshes, the convergence curves are plotted in Figure 9, and the errors and convergence rates are summarized in the Table 8 and Table 9. Same comments as for the convergence test case of the previous section hold.

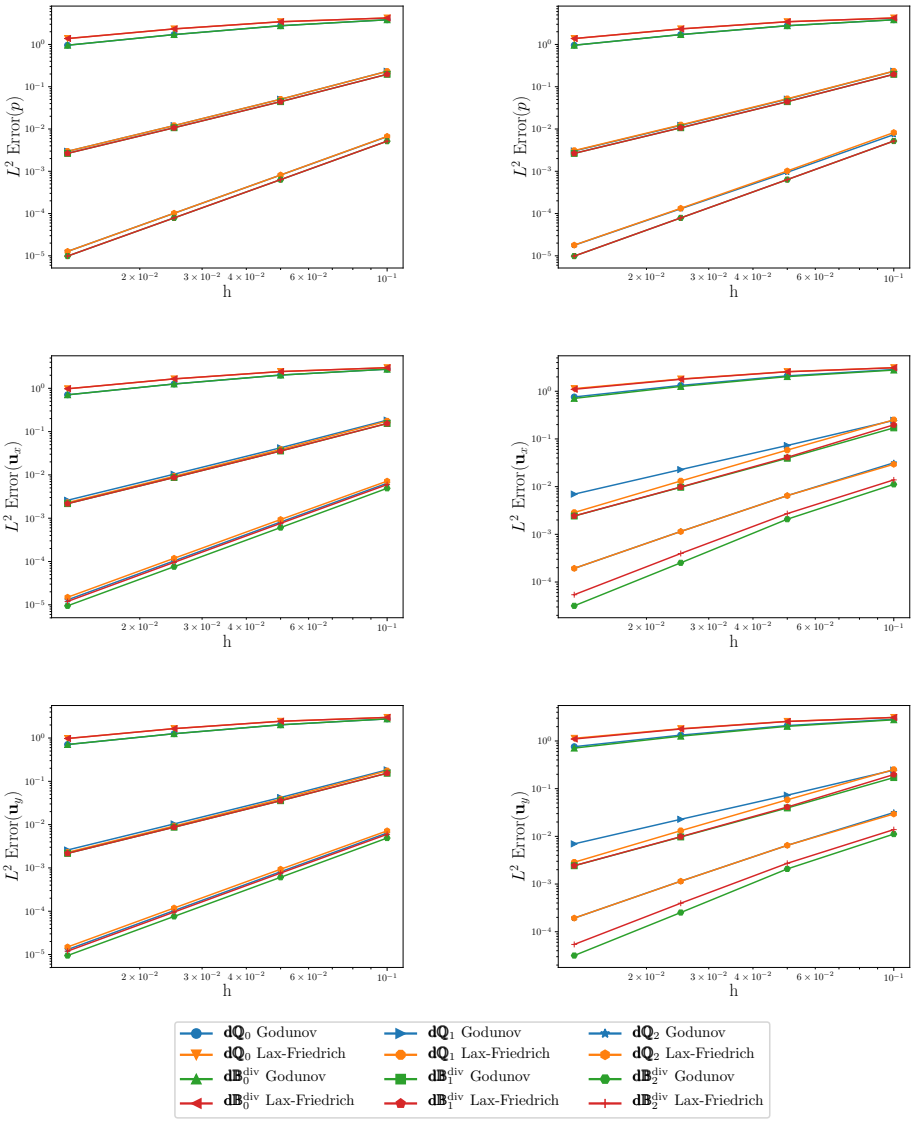

Figure 8: Error obtained on the test case described in subsubsection 6.2.2 with initial condition (31) on the left, and with the initial condition (32) added to (31) on the right, on a series of Cartesian meshes. For each of the test cases, the error obtained for the variables p (top row), $\mathbf{u}_x$ (middle row) and $\mathbf{u}_y$ (bottom row) is shown for different approximation spaces and for the Lax-Friedrich and Godunov flux.

	Godunov				Lax-Friedrich			
	$\mathbf{d}\mathbb{Q}_0$		$\mathbf{d}\mathbb{B}_0^{\text{div}}$		$\mathbf{d}\mathbb{Q}_0$		$\mathbf{d}\mathbb{B}_0^{\text{div}}$	
h	Error	rate	Error	rate	Error	rate	Error	rate
0.1	2.85e+00		2.78e+00		3.12e+00		3.11e+00	
0.05	2.10e+00	0.44	2.03e+00	0.46	2.58e+00	0.27	2.56e+00	0.28
0.025	1.33e+00	0.66	1.26e+00	0.69	1.81e+00	0.51	1.78e+00	0.52
0.0125	7.59e-01	0.81	7.09e-01	0.83	1.14e+00	0.67	1.10e+00	0.70
	Godunov				Lax-Friedrich			
	$\mathbf{d}\mathbb{Q}_1$		$\mathbf{d}\mathbb{B}_1^{\text{div}}$		$\mathbf{d}\mathbb{Q}_1$		$\mathbf{d}\mathbb{B}_1^{\text{div}}$	
h	Error	rate	Error	rate	Error	rate	Error	rate
0.1	2.45e-01		1.71e-01		2.52e-01		1.98e-01	
0.05	7.29e-02	1.75	3.94e-02	2.12	5.84e-02	2.11	4.11e-02	2.26
0.025	2.28e-02	1.68	9.70e-03	2.02	1.31e-02	2.15	9.83e-03	2.07
0.0125	6.96e-03	1.71	2.42e-03	2.00	2.87e-03	2.20	2.43e-03	2.02
	Godunov				Lax-Friedrich			
	$\mathbf{d}\mathbb{Q}_2$		$\mathbf{d}\mathbb{B}_2^{\text{div}}$		$\mathbf{d}\mathbb{Q}_2$		$\mathbf{d}\mathbb{B}_2^{\text{div}}$	
h	Error	rate	Error	rate	Error	rate	Error	rate
0.1	3.15e-02		1.12e-02		2.94e-02		1.38e-02	
0.05	6.47e-03	2.29	2.07e-03	2.43	6.48e-03	2.18	2.72e-03	2.35
0.025	1.15e-03	2.50	2.53e-04	3.04	1.14e-03	2.50	3.96e-04	2.78
0.0125	1.93e-04	2.57	3.17e-05	3.00	1.93e-04	2.57	5.41e-05	2.87

Table 7: Errors and convergence rates obtained on the variable $\mathbf{u}_x$ with the test case described in subsubsection 6.2.2 with initial condition (31), on a series of Cartesian meshes. Results show a high benefit in using the space $\mathbf{d}\mathbb{B}_k^{\text{curl}}$ with the Godunov flux, which is the only one to always reach the optimal order.

	Godunov		Lax-Friedrich	
h	Error	rate	Error	rate
0.08439823	2.39e+00		2.70e+00	
0.04187874	1.58e+00	0.59	1.94e+00	0.47
0.02226197	9.29e-01	0.84	1.20e+00	0.77
0.01091023	4.93e-01	0.89	6.58e-01	0.84
	Godunov		Lax-Friedrich	
h	Error	rate	Error	rate
0.08439823	1.43e-01		1.55e-01	
0.04187874	2.94e-02	2.26	3.15e-02	2.27
0.02226197	6.48e-03	2.39	7.41e-03	2.29
0.01091023	1.53e-03	2.03	1.97e-03	1.86
	Godunov		Lax-Friedrich	
h	Error	rate	Error	rate
0.08439823	7.62e-03		8.87e-03	
0.04187874	9.12e-04	3.03	1.28e-03	2.76
0.02226197	1.09e-04	3.35	1.78e-04	3.12
0.01091023	1.30e-05	2.98	2.49e-05	2.76

Table 8: Errors and convergence rates obtained on the variable $\mathbf{u}_x$ with the test case described in subsubsection 6.2.2 with initial condition (31), on the series of triangular meshes. Results show a low benefit in using the Godunov flux, namely in exactly preserving the divergence.

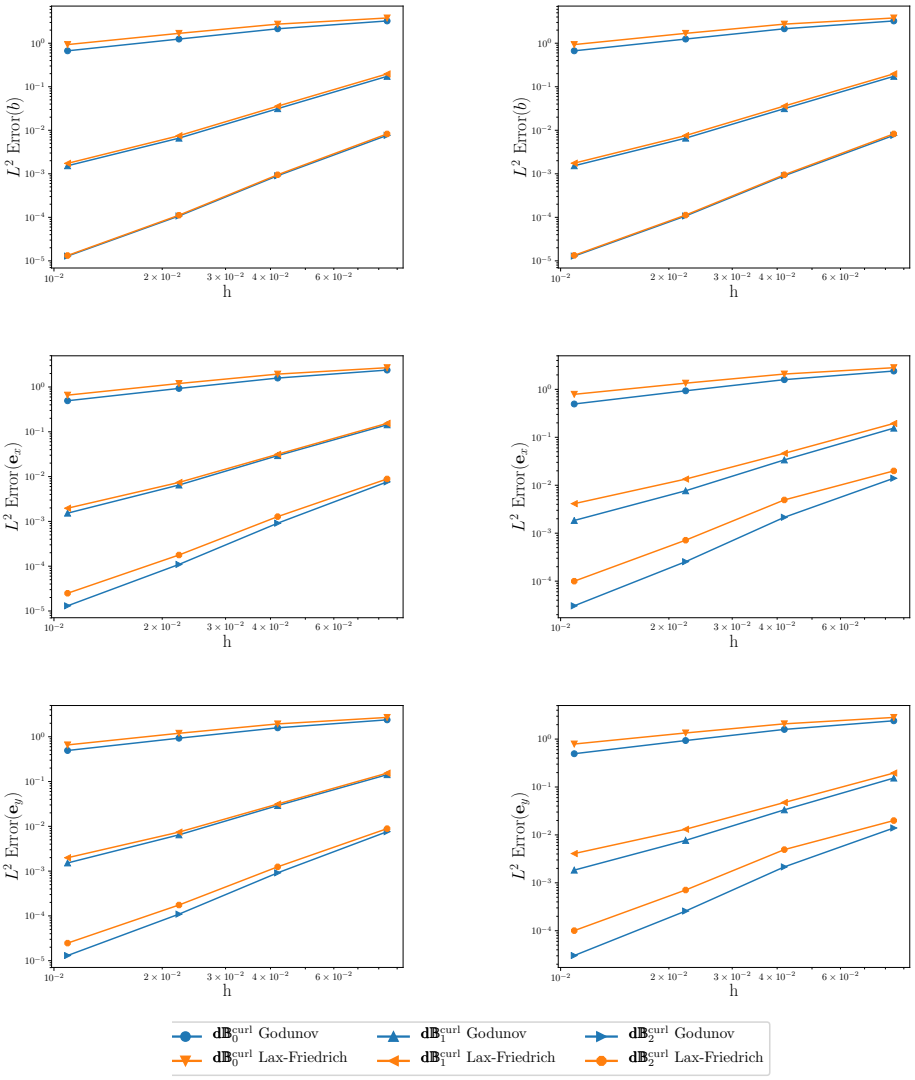

Figure 9: Error obtained on the test case described in subsubsection 6.2.2 with initial condition (31) on the left, and with the initial condition (32) added to (31) on the right, on a series of unstructured triangular meshes. For each of the test cases, the error obtained for the variables p (top row), $\mathbf{u}_x$ (middle row) and $\mathbf{u}_y$ (bottom row) is shown for different degrees, and for the Lax-Friedrich and Godunov numerical flux.

	Godunov		Lax-Friedrich	
h	Error	rate	Error	rate
0.08439823	2.41e+00		2.83e+00	
0.04187874	1.59e+00	0.59	2.08e+00	0.43
0.02226197	9.33e-01	0.85	1.34e+00	0.69
0.01091023	4.95e-01	0.89	7.87e-01	0.75
	Godunov		Lax-Friedrich	
h	Error	rate	Error	rate
0.08439823	1.55e-01		1.94e-01	
0.04187874	3.37e-02	2.18	4.63e-02	2.05
0.02226197	7.66e-03	2.34	1.34e-02	1.96
0.01091023	1.84e-03	2.00	4.13e-03	1.65
	Godunov		Lax-Friedrich	
h	Error	rate	Error	rate
0.08439823	1.40e-02		1.99e-02	
0.04187874	2.14e-03	2.68	4.94e-03	1.99
0.02226197	2.54e-04	3.37	7.14e-04	3.06
0.01091023	3.06e-05	2.97	9.98e-05	2.76

Table 9: Errors and convergence rates obtained on the variable $\mathbf{u}_x$ with the test case described in subsubsection 6.2.2 with initial condition (31), on the series of triangular meshes. Results show a higher benefit than in Table 8 in using the Godunov flux for preserving exactly the divergence.

6.3 Induction equation

In this section, we are interested in the system (20). The test case is taken from [66, Section 4.3] *Rotating discontinuous magnetic field loop*, still, it was modified in order to ensure that the magnetic loop is regular because we wish to do a convergence study. The computational domain is still $[0,1]^2$, and the vector field $\mathbf{v}$ is an orthoradial velocity with respect to the center of the computational domain $(0.5, 0.5)$: $\mathbf{v} = -\mathbf{e}_\theta$.

The initial condition is defined by

$$\mathbf{u}^0(\mathbf{x}) = \begin{cases} \text{if } \overline{r} < r_0 & \begin{cases} \mathbf{u}_x = -2K_0\alpha\overline{y}\,\dfrac{\mathrm{e}^{-\alpha/(1-\overline{r}^2)}}{(1-\overline{r})^2} \\ \mathbf{u}_y = \quad 2K_0\alpha\overline{x}\,\dfrac{\mathrm{e}^{-\alpha/(1-\overline{r}^2)}}{(1-\overline{r})^2} \end{cases} \\ \text{if } \overline{r} \geq r_0 & 0, \end{cases}$$

where $r^2 = (x-x_c)^2 + (y-y_c)^2$, $\overline{r} = r/r_0$, $\overline{x} = x/r_0$, $\overline{y} = y/r_0$, and K_0, α, x_c, y_c and r_0 are numerical parameters of the test case. This solution is such that $\mathbf{u}^0 = \nabla^\perp f^0$, where f^0 is the regular function

$$f^0(\mathbf{x}) := \begin{cases} -K_0\overline{r}_0\mathrm{e}^{-\alpha/(1-\overline{r}^2)} & \text{if } \overline{r} < \overline{r}_0 \\ 0 & \text{otherwise.} \end{cases}$$

The initial solution is a vortex rotating around the point (x_c, y_x). The field $\mathbf{v}$ induces a rotation of the solution around $(0.5, 0.5)$, which means that the exact solution is a vortex rotating around its center, and the center of the vortex rotates around $(0.5, 0.5)$ with angular velocity equal to 1, namely

$$\mathbf{u}(\mathbf{x}, t) = R(-t)\mathbf{u}^0\left(R(t)\mathbf{x}\right),$$

where $R(t)$ is the matrix of rotation around $(0.5, 0.5)$ of angle t:

$$R(t) := \begin{pmatrix} \cos t & -\sin t \\ \sin t & \cos t \end{pmatrix}.$$

degree	0	1	2
Triangular	0	$2.9602e-14$	$9.43413e-14$
Cartesian	0	0	0
Unstructured quad	0	$4.26275e-14$	$1.69086e-13$

Table 10: L^2 norm of the initial divergence when the initial condition is computed as in Remark 6 for the different meshes of Figure 3 and for degree 0, 1 and 2.

degree 0	Cartesian				Triangle				
		$\mathbf{u}_x$		$\mathbf{u}_y$			$\mathbf{u}_x$		$\mathbf{u}_y$	
	h	Error	rate	Error	rate	h	Error	rate	Error	rate
	1.00e-01	6.15e-03		5.84e-03		8.44e-02	6.71e-03		5.43e-03	
	5.00e-02	5.07e-03	0.28	4.57e-03	0.35	4.19e-02	4.72e-03	0.50	4.67e-03	0.22
	2.50e-02	3.15e-03	0.69	2.83e-03	0.69	2.23e-02	2.84e-03	0.81	2.72e-03	0.85
	1.25e-02	1.69e-03	0.90	1.50e-03	0.92	1.09e-02	1.61e-03	0.80	1.49e-03	0.84
degree 1	Cartesian				Triangle				
		$\mathbf{u}_x$		$\mathbf{u}_y$			$\mathbf{u}_x$		$\mathbf{u}_y$	
	h	Error	rate	Error	rate	h	Error	rate	Error	rate
	1.00e-01	2.42e-03		2.47e-03		8.44e-02	3.80e-03		3.85e-03	
	5.00e-02	1.29e-03	0.90	8.24e-04	1.58	4.19e-02	1.94e-03	0.96	1.48e-03	1.37
	2.50e-02	6.01e-04	1.11	1.93e-04	2.10	2.23e-02	1.02e-03	1.01	4.96e-04	1.73
	1.25e-02	2.26e-04	1.41	4.17e-05	2.21	1.09e-02	3.11e-04	1.67	1.71e-04	1.49
degree 2	Cartesian				Triangle				
		$\mathbf{u}_x$		$\mathbf{u}_y$			$\mathbf{u}_x$		$\mathbf{u}_y$	
	h	Error	rate	Error	rate	h	Error	rate	Error	rate
	1.00e-01	1.57e-03		1.20e-03		8.44e-02	3.21e-03		2.29e-03	
	5.00e-02	3.39e-04	2.21	2.09e-04	2.52	4.19e-02	8.45e-04	1.91	5.59e-04	2.01
	2.50e-02	5.53e-05	2.62	2.59e-05	3.01	2.23e-02	1.32e-04	2.94	8.35e-05	3.01
	1.25e-02	5.29e-06	3.39	2.41e-06	3.42	1.09e-02	2.43e-05	2.37	1.56e-05	2.35

Table 11: Errors obtained for the test case of the Rotating regular magnetic loop on triangular and quadrangular meshes. The error obtained is close of the optimal rate of convergence.

The computations are led with the approximation space $\mathbf{dI\!B}_k^{\mathrm{curl}}$, and with the Godunov' flux. The initial condition is computed with the method explained in Remark 6.

6.3.1 Conservation of the divergence free field

We first check that the divergence of $\mathbf{u}$ is preserved, equal to 0. For this, the test case is run until time $t = \pi$ on the different meshes shown in Figure 3. The initial L^2 norm of $\nabla^\star \mathbf{u}^0$ is summarized in Table 10. Results show that the method described in Remark 6 ensures the zero divergence for the initial condition.

The difference with respect to the initial divergence is plotted in Figure 10, and show preservation up to round-off errors of the divergence free field.

6.3.2 Convergence test

We wish now to perform a convergence test on the series of Cartesian and unstructured triangular meshes described in the beginning of the section. In this test, the computation is led until $t = 0.5$. The convergence curves for the two variables $\mathbf{u}_x$ and $\mathbf{u}_y$ are plotted in Figure 11, whereas the convergence rate computations are shown in Table 11. Both the table and the figure represent a convergence close of the optimal order of convergence.

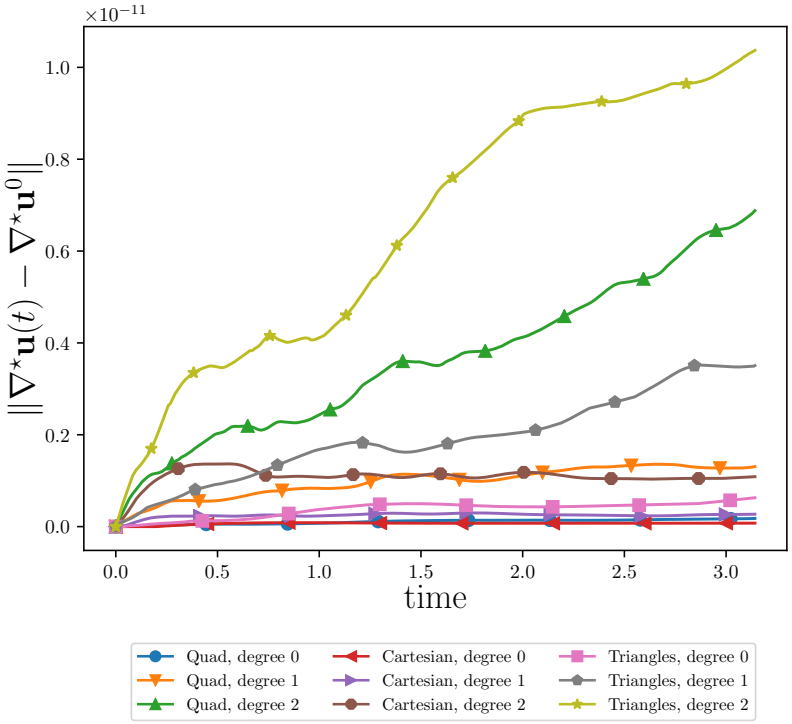

Figure 10: Time evolution of $\|\nabla^\star \mathbf{u} - \nabla^\star \mathbf{u}^0\|_2$ with respect to the time for a coarse Cartesian, unstructured quadrangular and a triangular mesh (all shown in Figure 3). Note that the scale is 10^{-11}, so that the figure shows exact (up to round-off errors) preservation of the divergence.

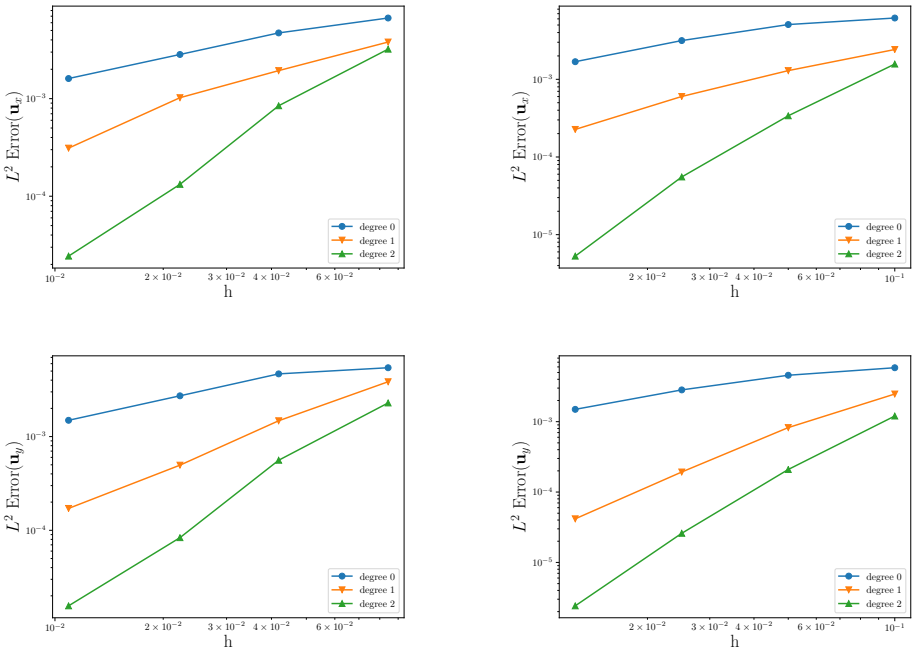

Figure 11: Error curves for the test case described in subsubsection 6.3.2. The top figures are the error on $\mathbf{u}_x$, whereas the bottom figures are the error on $\mathbf{u}_y$. The left column matches with triangular meshes whereas the right column is for Cartesian meshes.

7 Conclusion

In this article, the discrete preservation of differential constraints was investigated for the discontinuous Galerkin methods. The method developed within this article relies on a previously proposed framework for deriving appropriate approximation spaces for vectors, which fits in a discrete de-Rham context [54]. Based on this framework, we were able to propose a discrete version of the Hodge star operators, exterior derivative and the adjoint of the exterior derivative. For a continuous equation on a vector that preserves either the curl or the divergence, we were able to prove that the classical discontinuous Galerkin method preserves also this constraint at the discrete level under the following assumptions:

- Use the correct approximation space for vector unknowns
- Use a numerical flux which diffusion is either parallel (for preserving a curl) or orthogonal (for preserving a divergence) to the normal of the faces.

Notably, the curl or the divergence that are preserved are defined in an adjoint sense, namely they are exterior co-derivative. This use of the adjoint de-Rham complex is in fact very well suited with the fact that our numerical method is of Galerkin' type. Indeed, taking the strong exterior derivative of the solution of a numerical scheme seems to be a tedious task in general. On the contrary, taking the adjoint of the exterior derivative is a very simple operation for a Galerkin based numerical scheme: it just consists in testing the weak formulation with a gradient or a curl of a function. For the induction equation, it was even possible to derive a discrete transport equation in the space $\mathbb{A}_{k+1}$ for the adjoint divergence, starting from the discontinuous Galerkin method in $\mathbf{d}\mathbb{B}_k^{\mathrm{curl}}$ for the unknown vector. Last, the clear discrete de-Rham framework that was developed in this article allows to initialize easily a divergence free or a curl free field from the knowledge of its potential.

Numerical tests were performed on three linear systems: the two dimensional Maxwell system for the conservation of the divergence, the two dimensional wave system for the conservation of the curl, and the two dimensional induction equation. Numerical tests confirmed the theoretical results, and show also that the theoretical results seem to be sharp, in the sense that if one of the hypothesis of Proposition 5 and Proposition 4 is not ensured (wrong approximation space or diffusion not in the right direction), the conservation of the curl or the divergence is jeopardized.

Note that the numerical tests were performed only on linear systems, but the propositions that were proven hold also for nonlinear problems. Also, the implementation was done with a special family of finite elements on quads (and also on triangles), but theoretical results hold for other finite elements proposed in [54].

Last, it is also important to see that Proposition 4 and Proposition 5 hold also in dimension 3, provided the right approximation spaces were derived. We are currently investigating the extension of the results of this article to dimension 3 and to nonlinear systems of conservation law.

References

[1] Douglas Norman Arnold. *Finite element exterior calculus*. SIAM, 2018.

[2] Douglas Norman Arnold, Richard Steven Falk, and Ragnar Winther. Finite element exterior calculus, homological techniques, and applications. *Acta numerica*, 15:1–155, 2006.

[3] Douglas Norman Arnold, Richard Steven Falk, and Ragnar Winther. Finite element exterior calculus: from Hodge theory to numerical stability. *Bulletin of the American mathematical society*, 47(2):281–354, 2010.

[4] Douglas Norman Arnold and Anders Bernhard Logg. Periodic table of the finite elements. *SIAM News*, 47(9):212, 2014.

[5] Dinshaw S. Balsara. Divergence-free adaptive mesh refinement for magnetohydrodynamics. *Journal of Computational Physics*, 174(2):614–648, 2001.

[6] Dinshaw S. Balsara. Second-order-accurate schemes for magnetohydrodynamics with divergence-free reconstruction. *The Astrophysical Journal Supplement Series*, 151(1):149, 2004.

[7] Dinshaw S. Balsara and Daniel Shields Spicer. A staggered mesh algorithm using high order Godunov fluxes to ensure solenoidal magnetic fields in magnetohydrodynamic simulations. *Journal of Computational Physics*, 149(2):270–292, 1999.

[8] Wasilij Barsukow. Stationarity preserving schemes for multi-dimensional linear systems. *Mathematics of Computation*, 88(318):1621–1645, 2019.

[9] Wasilij Barsukow. Truly multi-dimensional all-speed schemes for the Euler equations on Cartesian grids. *Journal of Computational Physics*, 435:110216, 2021.

[10] Lourenco Beirão da Veiga, Franco Brezzi, Andrea Cangiani, Gianmarco Manzini, Luisa Donatella Marini, and Alessandro Russo. Basic principles of virtual element methods. *Mathematical Models and Methods in Applied Sciences*, 23(01):199–214, 2013.

[11] John B. Bell, Phillip Colella, and Harland M. Glaz. A second-order projection method for the incompressible Navier-Stokes equations. *Journal of computational physics*, 85(2):257–283, 1989.

[12] Jérôme Bonelle. *Compatible Discrete Operator schemes on polyhedral meshes for elliptic and Stokes equations*. PhD thesis, Université Paris-Est, 2014.

[13] Jérôme Bonelle and Alexandre Ern. Analysis of compatible discrete operator schemes for the Stokes equations on polyhedral meshes. *IMA Journal of numerical analysis*, 35(4):1672–1697, 2015.

[14] Walter Boscheri, Raphaël Loubère, and Pierre-Henri Maire. An unconventional divergence preserving finite-volume discretization of Lagrangian ideal MHD. *Communications on Applied Mathematics and Computation*, pages 1–55, 2023.

[15] Alain Bossavit. Whitney forms: A class of finite elements for three-dimensional computations in electromagnetism. *IEE Proceedings A (Physical Science, Measurement and Instrumentation, Management and Education, Reviews)*, 135(8):493–500, 1988.

[16] Alain Bossavit. *Computational electromagnetism: variational formulations, complementarity, edge elements*. Academic Press, 1998.

[17] Alain Bossavit. On the geometry of electromagnetism (4): Maxwell's house. *AEM Journal of the Japan Society of Applied Electromagnetics and Mechanics*, 6(4):318–326, 1998.

[18] Jeremiah U. Brackbill and Daniel C. Barnes. The effect of nonzero $\nabla \cdot B$ on the numerical solution of the magnetohydrodynamic equations. *Journal of Computational Physics*, 35(3):426–430, 1980.

[19] Henri Cartan. *Differential forms*. Hermann, 1967.

[20] Andreas Dedner, Friedemann Kemm, Dietmar Kröner, Claus-Dieter Munz, Thomas Schnitzer, and Matthias Wesenberg. Hyperbolic divergence cleaning for the MHD equations. *Journal of Computational Physics*, 175(2):645–673, 2002.

[21] Stéphane Dellacherie, Pascal Omnes, and Felix Rieper. The influence of cell geometry on the Godunov scheme applied to the linear wave equation. *Journal of Computational Physics*, 229(14):5315–5338, 2010.

[22] Daniele Antonio Di Pietro and Jérôme Droniou. *The Hybrid High-Order method for polytopal meshes*, volume 19. Modeling, Simulation and Application, Springer, 2020.

[23] Michael Dumbser, Francesco Fambri, Elena Gaburro, and Anne Reinarz. On GLM curl cleaning for a first order reduction of the CCZ4 formulation of the Einstein field equations. *Journal of Computational Physics*, 404:109088, 2020.

[24] Charles R. Evans and John F. Hawley. Simulation of magnetohydrodynamic flows-a constrained transport method. *Astrophysical Journal, Part 1 (ISSN 0004-637X), vol. 332, Sept. 15, 1988, p. 659-677.*, 332:659–677, 1988.

[25] Robert Eymard, Thierry Gallouët, Raphaele Herbin, and Jean-Claude Latché. Convergence of the MAC scheme for the compressible Stokes equations. *SIAM Journal on Numerical Analysis*, 48(6):2218–2246, 2010.

[26] Robert Eymard, Thierry Gallouët, Raphaele Herbin, and Jean-Claude Latché. A convergent finite element-finite volume scheme for the compressible Stokes problem. part II: the isentropic case. *Mathematics of Computation*, 79(270):649–675, 2010.

[27] Franz Georg Fuchs, Kenneth Aksel Hvistendahl Karlsen, Siddharta Mishra, and Nils Henrik Risebro. Stable upwind schemes for the magnetic induction equation. *ESAIM: Mathematical Modelling and Numerical Analysis-Modélisation Mathématique et Analyse Numérique*, 43(5):825–852, 2009.

[28] Thierry Gallouët, Raphaele Herbin, and Jean-Claude Latché. A convergent finite element-finite volume scheme for the compressible Stokes problem. part I: The isothermal case. *Mathematics of Computation*, 78(267):1333–1352, 2009.

[29] Sergei Konstantinovich Godunov. An interesting class of quasi-linear systems. In *Doklady Akademii Nauk*, volume 139-3, pages 521–523. Russian Academy of Sciences, 1961.

[30] Sergueï Konstantinovitch Godunov. Symmetric form of the magnetohydrodynamic equation. Technical report, Computer Center, Novosibirsk, USSR, 1972.

[31] Sigal Gottlieb, David I. Ketcheson, and Chi-Wang Shu. High order strong stability preserving time discretizations. *Journal of Scientific Computing*, 38(3):251–289, 2009.

[32] Hervé Guillard. On the behavior of upwind schemes in the low Mach number limit. IV: P0 approximation on triangular and tetrahedral cells. *Computers & Fluids*, 38(10):1969–1972, 2009.

[33] Hervé Guillard and Boniface Nkonga. On the behaviour of upwind schemes in the low Mach number limit: A review. *Handbook of Numerical Analysis*, 18:203–231, 2017.

[34] Allen Hatcher. *Algebraic Topology*. Cambridge University Press, 2001.

[35] Christiane Helzel, James Alexander Rossmanith, and Bertram Taetz. An unstaggered constrained transport method for the 3d ideal magnetohydrodynamic equations. *Journal of Computational Physics*, 230(10):3803–3829, 2011.

[36] Holger Heumann and Ralf Hiptmair. Eulerian and semi-Lagrangian methods for convection-diffusion for differential forms. *Discrete and Continuous Dynamical Systems*, 29(4):1471–1495, 2011.

[37] Holger Heumann and Ralf Hiptmair. Stabilized Galerkin methods for magnetic advection. *ESAIM: Mathematical Modelling and Numerical Analysis-Modélisation Mathématique et Analyse Numérique*, 47(6):1713–1732, 2013.

[38] Holger Heumann, Ralf Hiptmair, Kun Li, and Jinchao Xu. Fully discrete semi-Lagrangian methods for advection of differential forms. *BIT Numerical Mathematics*, 52(4):981–1007, 2012.

[39] Ralf Hiptmair. Discrete Hodge operators. *Numerische Mathematik*, 90:265–289, 2001.

[40] Ralf Hiptmair. Finite elements in computational electromagnetism. *Acta Numerica*, 11:237–339, 2002.

[41] James Mac Hyman and Mikhail Shashkov. Natural discretizations for the divergence, gradient, and curl on logically rectangular grids. *Computers & Mathematics with Applications*, 33(4):81–104, 1997.

[42] Rolf Jeltsch and Manuel Torrilhon. On curl-preserving finite volume discretizations for shallow water equations. *BIT Numerical Mathematics*, 46:35–53, 2006.

[43] Jonathan Jung and Vincent Perrier. Behavior of the discontinuous Galerkin method for compressible flows at low Mach number on triangles and tetrahedrons. *SIAM Journal on Scientific Computing*, 46(1):A452–A482, 2024.

[44] Vyacheslav Ivanovich Lebedev. Difference analogues of orthogonal decompositions, basic differential operators and some boundary problems of mathematical physics. I. *USSR Computational Mathematics and Mathematical Physics*, 4(3):69–92, 1964.

[45] Martin Werner Licht. Complexes of discrete distributional differential forms and their homology theory. *Foundations of Computational Mathematics*, 17(4):1085–1122, 2017.

[46] Konstantin Lipnikov, Gianmarco Manzini, and Mikhail Shashkov. Mimetic finite difference method. *Journal of Computational Physics*, 257:1163–1227, 2014.

[47] Riccardo Milani, Jérôme Bonelle, and Alexandre Ern. Artificial compressibility methods for the incompressible Navier–Stokes equations using lowest-order face-based schemes on polytopal meshes. *Computational Methods in Applied Mathematics*, 22(1):133–154, 2022.

[48] Siddhartha Mishra and Magnus Svärd. On stability of numerical schemes via frozen coefficients and the magnetic induction equations. *BIT Numerical Mathematics*, 50:85–108, 2010.

[49] Claus-Dieter Munz, Pascal Omnes, Rudolf Schneider, Éric Sonnendrücker, and Ursula Voss. Divergence correction techniques for Maxwell solvers based on a hyperbolic model. *Journal of Computational Physics*, 161(2):484–511, 2000.

[50] Jean-Claude Nédélec. Mixed finite elements in $\mathbb{R}^3$. *Numerische Mathematik*, 35:315–341, 1980.

[51] Roy Nicolaides and X. Wu. Analysis and convergence of the MAC scheme. II. Navier-Stokes equations. *Mathematics of Computation*, 65(213):29–44, 1996.

[52] Roy A. Nicolaides. Analysis and convergence of the MAC scheme. I. the linear problem. *SIAM Journal on Numerical Analysis*, 29(6):1579–1591, 1992.

[53] Cecilia Pagliantini. *Computational magnetohydrodynamics with discrete differential forms.* PhD thesis, ETH Zurich, 2016.

[54] Vincent Perrier. discrete de-Rham complex involving a discontinuous finite element space for velocities: the case of periodic straight triangular and Cartesian meshes. *Submitted*, 2024. Available at https://inria.hal.science/hal-04564069.

[55] Kenneth Grant Powell. An approximate Riemann solver for magnetohydrodynamics (that works in more than one dimension). Technical Report 94-24, ICASE, 1994.

[56] Kenneth Grant Powell, Philip L. Roe, Timur J. Linde, Tamas I. Gombosi, and Darren L. De Zeeuw. A solution-adaptive upwind scheme for ideal magnetohydrodynamics. *Journal of Computational Physics*, 154(2):284–309, 1999.

[57] Pierre-Arnaud Raviart and Jean-Marie Thomas. A mixed finite element method for 2-nd order elliptic problems. In *Mathematical aspects of finite element methods*, pages 292–315. Springer, 1977.

[58] Pierre-Arnaud Raviart and Jean-Marie Thomas. Primal hybrid finite element methods for 2nd order elliptic equations. *Mathematics of Computation*, 31(138):391–413, 1977.

[59] Laura Río-Martín, Firas Dhaouadi, and Michael Dumbser. An exactly curl-free finite-volume scheme for a hyperbolic compressible barotropic two-phase model. *arXiv preprint arXiv:2403.18724*, 2024.

[60] Evgeniy Romensky. Hyperbolic systems of thermodynamically compatible conservation laws in continuum mechanics. *Mathematical and computer modelling*, 28(10):115–130, 1998.

[61] Maurizio Tavelli and Michael Dumbser. A pressure-based semi-implicit space–time discontinuous Galerkin method on staggered unstructured meshes for the solution of the compressible Navier–Stokes equations at all Mach numbers. *Journal of Computational Physics*, 341:341–376, 2017.

[62] Romain Teyssier and Benoît Commerçon. Numerical methods for simulating star formation. *Frontiers in Astronomy and Space Sciences*, 6:51, 2019.

[63] Manuel Torrilhon. Locally divergence-preserving upwind finite volume schemes for magnetohydrodynamic equations. *SIAM Journal on Scientific Computing*, 26(4):1166–1191, 2005.

[64] Manuel Torrilhon and Michael Fey. Constraint-preserving upwind methods for multidimensional advection equations. *SIAM Journal on numerical analysis*, 42(4):1694–1728, 2004.

[65] Gábor Tóth. The $\nabla \cdot B = 0$ constraint in shock-capturing magnetohydrodynamics codes. *Journal of Computational Physics*, 161(2):605–652, 2000.

[66] Maria Han Veiga, David Aarón Velasco-Romero, Quentin Wenger, and Romain Teyssier. An arbitrary high-order spectral difference method for the induction equation. *Journal of Computational Physics*, 438:110327, 2021.

[67] Hassler Whitney. *Geometric integration theory*. Princeton University Press, Princeton, NJ, 1957.

[68] Kane Yee. Numerical solution of initial boundary value problems involving Maxwell's equations in isotropic media. *IEEE Transactions on antennas and propagation*, 14(3):302–307, 1966.

A Summary of the operators on differential forms and on their proxies

In the following table, the proxy of the different operators used in this article are summarized, when the choice of proxy for Λ^1 is (1).

k	0	1	2
Element of Λ^k	$\mathfrak{f}$	$\mathfrak{u}$	$\mathfrak{f}$
Proxy	f	$\mathbf{u}$	f
Proxy$(\bigstar_{\{k\}})$	f	$\mathbf{u}^\perp$	f
Proxy(d^k)	∇f	$\nabla^\perp \cdot \mathbf{u}$	–
Proxy(δ^k)	–	$-\nabla \cdot \mathbf{u}$	$-\nabla^\perp f$
Proxy $\left(\delta^{k+1}\mathrm{d}^k + \mathrm{d}^{k-1}\delta^k\right)$	$-\nabla \cdot (\nabla f)$	$-\nabla (\nabla \cdot \mathbf{u}) - \nabla^\perp \left(\nabla^\perp \cdot \mathbf{u}\right)$	$-\nabla^\perp \cdot \left(\nabla^\perp f\right)$
Proxy$(i_{\mathbf{b}})$	–	$\mathbf{b} \cdot \mathbf{u}$	$\mathbf{b}^\perp f$
Proxy$(j_{\mathbf{b}})$	$f\mathbf{b}$	$-\mathbf{u}^\perp \cdot \mathbf{b}$	–
Proxy$(\mathrm{L}_{\mathbf{b}})$	$\mathbf{b} \cdot \nabla f$	$\nabla (\mathbf{b} \cdot \mathbf{u}) + \mathbf{b}^\perp \nabla^\perp \cdot \mathbf{u}$	$\nabla \cdot (f\mathbf{b})$
Proxy$(\mathcal{L}_{\mathbf{b}})$	$-\nabla \cdot (f\mathbf{b})$	$-\nabla^\perp (\det(\mathbf{b}, \mathbf{u})) - \mathbf{b}\nabla \cdot \mathbf{u}$	$-\mathbf{b} \cdot \nabla f$

In the next table, the proxy of the different operators used in this article are summarized, when the choice of proxy for Λ^1 is (2).

k	0	1	2
Element of Λ^k	$\mathfrak{f}$	$\mathfrak{u}$	$\mathfrak{f}$
Proxy$^\perp$	f	$\mathbf{u}$	f
Proxy$^\perp(\bigstar_{\{k\}})$	f	$\mathbf{u}^\perp$	f
Proxy$^\perp(\mathrm{d}^k)$	$\nabla^\perp f$	$-\nabla \cdot \mathbf{u}$	–
Proxy$^\perp(\delta^k)$	–	$-\nabla^\perp \cdot \mathbf{u}$	∇f
Proxy$^\perp \left(\delta^{k+1}\mathrm{d}^k + \mathrm{d}^{k-1}\delta^k\right)$	$-\nabla^\perp \cdot \left(\nabla^\perp f\right)$	$-\nabla (\nabla \cdot \mathbf{u}) - \nabla^\perp \left(\nabla^\perp \cdot \mathbf{u}\right)$	$-\nabla \cdot (\nabla f)$
Proxy$^\perp(i_{\mathbf{b}})$	–	$\det(\mathbf{b}, \mathbf{u})$	$-f\mathbf{b}$
Proxy$^\perp(j_{\mathbf{b}})$	$f\mathbf{b}^\perp$	$-\mathbf{u} \cdot \mathbf{b}$	–
Proxy$^\perp(\mathrm{L}_{\mathbf{b}})$	$\mathbf{b} \cdot \nabla f$	$\nabla^\perp (\det(\mathbf{b}, \mathbf{u})) + \mathbf{b}\nabla \cdot \mathbf{u}$	$\nabla \cdot (f\mathbf{b})$
Proxy$^\perp(\mathcal{L}_{\mathbf{b}})$	$-\nabla \cdot (f\mathbf{b})$	$-\nabla (\mathbf{b} \cdot \mathbf{u}) - \mathbf{b}^\perp \nabla^\perp \cdot \mathbf{u}$	$-\mathbf{b} \cdot \nabla f$

Last, the effect of the exterior product on the proxies does not depend on the choice of proxies, and was summarized in Table 1.